Brain asymmetries from midlife to old adulthood and hemispheric brain age

Max Korbmacher[1,2,3,✉], Dennis van der Meer[2,4], Dani Beck[2,5,6], Ann-Marie de Lange[2,7,8], Eli Eikefjord[1,3], Arvid Lundervold[1,3,9,10], Ole A. Andreassen[2,11], Lars T. Westlye[2,6,11], and Ivan I. Maximov[1,2,✉]

[1]Department of Health and Functioning, Western Norway University of Applied Sciences, Bergen, Norway
[2]NORMENT Centre for Psychosis Research, Division of Mental Health and Addiction, University of Oslo and Oslo University Hospital, Oslo, Norway
[3]Mohn Medical Imaging and Visualization Centre (MMIV), Bergen, Norway
[8]Department of Psychiatry, University of Oxford, Oxford, UK
[7]LREN, Centre for Research in Neurosciences - Department of Clinical Neurosciences, CHUV and University of Lausanne, Lausanne, Switzerland
[4]Faculty of Health, Medicine and Life Sciences, Maastricht University, Maastricht, Netherlands
[5]Department of Psychiatric Research, Diakonhjemmet Hospital, Oslo, Norway
[6]Department of Psychology, University of Oslo, Oslo, Norway
[9]Department of Radiology, Haukeland University Hospital, Bergen, Norway
[10]Department of Biomedicine, University of Bergen, Bergen, Norway
[11]KG Jebsen Centre for Neurodevelopmental Disorders, University of Oslo, Oslo, Norway

The human brain demonstrates structural and functional asymmetries which have implications for ageing and the development of mental and neurological diseases. We used a set of magnetic resonance imaging (MRI) metrics derived from structural and diffusion MRI data in N = 48,040 UK Biobank participants to evaluate age-related differences in brain asymmetry. Most regional grey and white matter metrics presented asymmetry, which appears lower at higher age. Informed by these results, we conducted *hemispheric brain age* (HBA) predictions from left/right multimodal MRI metrics, and compared HBA to conventional predictions using metrics from both hemispheres. We present that HBA is concordant to conventional brain age predictions but offers the advantage of supplying a general marker of brain asymmetry when setting left/right HBA into relationship to each other. Similar to brain asymmetries, this discrepancy between left/right HBA is lower at higher ages. The findings emphasise the value of further investigating the role of decreasing brain asymmetries at higher ages in brain ageing and disease development.

Brain Asymmetry | Laterality | Brain Age | Age Prediction | Magnetic Resonance Imaging

Correspondence: ***max.korbmacher@hvl.no, ivan.maximov@hvl.no***

DRAFT

Introduction

There are various structural and functional differences in brain architecture between the left and right hemispheres (1–6). Microstructural brain characteristics, such as white matter (WM) pathways or intra- and extra-neurite water organisation, might underlie the brain's functional lateralisation (7). Functional network difference has been associated with handedness (8). Both structural and functional brain asymmetry exhibit clinical importance as there are differences in brain asymmetry between healthy controls and various disease groups, including neurodegenerative diseases such as Alzheimer's disease (9, 10), Parkinson's disease (11), and psychiatric disease such as obsessive–compulsive disorder (4, 12, 13) and schizophrenia (14). In that context and particularly relevant from a lifespan-perspective, cortical thickness asymmetry decreases throughout ageing, with this alteration being potentially accelerated in the development of neurodegenerative disorders such as Alzheimer's Disease (9). Similarly, some studies suggest lower WM microstructure asymmetry at higher ages, indicated by intra-axonal water fraction (15), fractional anisotropy, or the apparent diffusion coefficient (16). Additional investigations into brain asymmetries' age-dependencies can provide a more comprehensive understanding of the influence of asymmetries on ageing and disease development.

Brain age is a developing integrative marker of brain health, particularly sensitive to neurodegenerative diseases (17, 18). Brain age refers to the predicted age in contrast to chronological age and is based on a set of scalar metrics derived from brain scans such as MR. To date, brain age has often been estimated using a global brain parametrisation such as the averaged scalar measures over particular anatomical regions or the whole brain (17–21). Hence, we refer to these whole-brain age predictions as global brain age (GBA). However, while brain age has been calculated for different brain regions (18, 22–24), the use of hemisphere-specific data is usually not being considered as a potential source of additional information. Yet, one study presents hemisphere-specific and region-specific brain ages containing useful clinical information about post-stroke cognitive improvement (22).

Previous results show that brain age prediction depends on the specific features used (25–27), rendering for example modality as important. Yet, the influence of hemispheric differences or brain asymmetry on the age predictions remains unclear. However, previously outlined brain asymmetries (1–6) might be informative for age predictions. One way of leveraging brain asymmetries into simple metrics is to estimate separate brain ages for each hemisphere (HBA) and to then compare the estimates. It remains unclear whether predictions from a single hemisphere lead to less accurate predictions due to the inclusion of less data and a potential attenuation of noise. At the same time, in the case of diffusion MRI (dMRI), different model-based diffusion features yield highly concordant brain age predictions, also when varying the number of included features (21). Finally, although the evidence is mixed on the influence of handedness on brain

asymmetry (28–31), differences in handedness are potentially reflected in brain structure, which would in turn influence age predictions differently when obtained from the left or right hemisphere only. Hence, handedness requires further examination as potential confounding effect when assessing asymmetry.

HBA, a new brain age measure, may propose more sensitive brain health markers than GBA, as age predictions can be compared between hemispheres to infer the integrity of each hemisphere and give a general estimate of brain asymmetry. Brain asymmetries are commonly observed using the Laterality Index (LI) (32). However, different ways of estimating asymmetry can introduce variability in its dependency with age (33), and covariates of brain age require further investigation (34, 35). To extend the existing brain age conceptualisation of using features across the whole brain and to maximise interpretability, we restrict brain age predictions to region-averaged and global features and not asymmetries of these features. Additionally, differences in the models' abilities to predict age from WM microstructure features derived from dMRI compared to T_1-weighted features (volume, surface area, thickness) need to be ruled out in order to validate both GBA and HBA.

Hence, in the present work, we tested first the preregistered hypotheses (written study and analysis plan prior data inspection and analyses (36, 37)) that the GBA and HBA depend on the used MRI modality (Hypothesis 1), disentangling whether the different grey matter (GM) and WM metrics and the degree of their asymmetry influences brain age predictions. We furthermore tested whether there was an effect of hemisphere (Hypothesis 2) and handedness (Hypothesis 3) on brain age predictions. Exploratory analyses included (a) revealing hemispheric differences between GM and WM features, (b) examining LI associations with age, including the LI of the brain features as well as left and right brain ages, and (c) testing the consistency of brain age-covariate associations (specifically, health-and-lifestyle factors, as these were previously associated with brain age (20, 26, 38–41)).

Methods

Sample characteristics. We obtained UK Biobank (UKB) data (42), including $N = 48,040$ T_1-weighted datasets, $N = 39,637$ dMRI datasets, resulting in $N = 39,507$ joined/multimodal datasets after exclusions were applied. Participant data were excluded when consent had been withdrawn, an ICD-10 diagnosis from categories F (presence of mental and behavioural disorder), G (disease of the nervous system), I (disease of the circulatory system), or stroke was present, and when datasets were not meeting quality control standards using the YTTRIUM method (43) for dMRI datasets and Euler numbers were larger than 3 standard deviations below the mean for T_1-weighted data (44). In brief, YTTRIUM (43) converts the dMRI scalar metric into 2D format using a structural similarity (45, 46) extension of each scalar map to their mean image in order to create a 2D distribution of image and diffusion parameters. These quality assessments are based on a 2-step clustering algorithm applied to identify subjects located outside of the main distribution. Data were collected at four sites, with the T_1-weighted data collected in Cheadle (58.41%), Newcastle (25.97%), Reading (15.48%), and Bristol (0.14%). Of these data, 52.00% were females, and the participants age range was from 44.57 to 83.71, mean = 64.86 ± 7.77, median = 65.38 ± 8.79. DMRI data were available from four sites: Cheadle (57.76%), Newcastle (26.12%), Reading (15.98%), and Bristol (0.14), with 52.19% female, and an age range of 44.57 to 82.75, mean = 64.63 ± 7.70, median = 65.16 ± 8.73. The multimodal sample ($N = 39,507$) was 52.22% female, with an age range of 44.57 to 82.75, mean = 64.62 ± 7.70, median = 65.15 ± 8.73.

MRI acquisition and post-processing. UKB MRI data acquisition procedures are described elsewhere (42, 47, 48). The raw T_1-weighted and dMRI data were processed accordingly. Namely, the dMRI data passed through an optimised pipeline (43). The pipeline includes corrections for noise (49), Gibbs ringing (50), susceptibility-induced and motion distortions, and eddy current artifacts (51). Isotropic 1 mm^3 Gaussian smoothing was carried out using FSL's (52, 53) *fslmaths*. Employing the multi-shell data, Diffusion Tensor Imaging (DTI) (54), Diffusion Kurtosis Imaging (DKI) (55) and White Matter Tract Integrity (WMTI) (56) metrics were estimated using Matlab 2017b code (https://github.com/NYU-DiffusionMRI/DESIGNER). Spherical mean technique (SMT) (57), and multi-compartment spherical mean technique (SMTmc) (58) metrics were estimated using original code (https://github.com/ekaden/smt) (57, 58). Estimates from the Bayesian Rotational Invariant Approach (BRIA) were evaluated by the original Matlab code (https://bitbucket.org/reisert/baydiff/src/master/) (59).

T_1-weighted images were processed using Freesurfer (version 5.3) (60) automatic *recon-all* pipeline for cortical reconstruction and subcortical segmentation of the T_1-weighted images (http://surfer.nmr.mgh.harvard.edu/fswiki) (61).

In total, we obtained 28 WM metrics from six diffusion approaches (DTI, DKI, WMTI, SMT, SMTmc, BRIA; see for overview in Supplement 11). In order to normalise all metrics, we used Tract-based Spatial Statistics (TBSS) (62), as part of FSL (52, 53). In brief, initially all brain-extracted (63) fractional anisotropy (FA) images were aligned to MNI space using non-linear transformation (FNIRT) (53). Following, the mean FA image and related mean FA skeleton were derived. Each diffusion scalar map was projected onto the mean FA skeleton using the TBSS procedure. In order to provide a quantitative description of diffusion metrics we used the John Hopkins University (JHU) atlas (64), and obtained 30 hemisphere-specific WM regions of interest (ROIs) based on a probabilistic WM atlas (JHU) (65) for each of the 28 metrics. For T_1-weighted data, we applied the Desikan-Killiany Atlas (66). Altogether, 840 dMRI features were derived per individual [28 metrics $\times$ (24 ROIs + 6 tracts)] for each hemisphere, and 117 T_1-weighted features (surface area, volume, thickness for each of the 34 regions; 3 whole-brain gray matter averages, and 2 averages of white matter surface area and

DRAFT

volume) for each hemisphere.

Brain Age Predictions. Brain age was predicted using the XGBoost algorithm (67) implemented in Python (v3.7.1). We used six data subsets to predict brain age split in the following manner: 1) right hemisphere T_1-weighted, 2) left hemisphere T_1-weighted, 3) left hemisphere diffusion, 4) right hemisphere diffusion, 5) left hemisphere multimodal, 6) right hemisphere multimodal. We applied nested k-fold cross-validation with 5 outer and 10 inner folds (see Supplement 1 for tuned hyperparameters). We corrected for age-bias and mere age-effects (68, 69) by including age in the regression equations (Eq. 4) when assessing effects of modality, hemisphere, and handedness on brain age, as well as phenotype associations with brain ages (Eq. 8).

Statistical Analyses. All statistical analyses were carried out using Python (v3.7.1) and R (v4.2.0).

Hemispheric differences and age sensitivity. To give an overview of the extent of brain asymmetry, we assessed the significance of T_1-weighted and dMRI features' asymmetry using two-sided t-tests. The lateralisation or asymmetry of the brain features was estimated as the following: we applied the LI (32) to both regional features and features averaged over each hemisphere (see also (33)).

$$LI = \frac{L-R}{L+R}, \tag{1}$$

where L and R belongs to any left and right scalar metric, respectively.
We then used linear regression models correcting for sex and scanning site to predict age from all regular and LI features:

$$Age = F + Sex + Site, \tag{2}$$

where F is a scalar metric such as, for example, hippocampus volume (derived from T_1-weighted image) or tapetum fractional anisotropy (derived from DTI).
Likelihood ratio tests (LRTs) (70) were used to assess the age sensitivity of all T_1-weighted and dMRI features and their asymmetry/LI features by comparing the above models with baseline models not including the respective feature:

$$Age = Sex + Site \tag{3}$$

We used the same procedure for region-averaged and hemispheric average metrics for regular and LI features. Hemispheric averages of regular features were then visualised by age, including surface area, volume, thickness for T_1-weighted data, and intra- and extra-axonal water diffusivities as well as for DTI and DKI metrics.

Brain age assessment. We estimated correlations across HBA and GBA to assess their similarities in addition to the model output provided from the prediction procedure. We also correlated age with the LI (see Eq. (1)) for the three modalities (dMRI, T_1-weighted, multimodal MRI), and estimated the age sensitivity of the LI as described in Eqs. (2-3).

As preregistered (https://aspredicted.org/if5yr.pdf), to test the relationships between hemisphere (H), modality (M), and HBA while controlling for age, sex and scanner site, we employed linear mixed effects regression (LMER) models of the following form:

$$\begin{aligned} HBA = H + M + H \times M + Sex + Age + \\ Sex \times Age + (1|Site) + (1|I), \end{aligned} \tag{4}$$

where I refers to the random intercept at the level of the individual. Post-hoc group differences were observed for hemisphere, modality and their interaction.
Next, handedness (Ha) was added to the model to observe whether there are model differences between the resulting LMER:

$$\begin{aligned} HBA = Ha + H \times Ha + H + M + H \times M + \\ Sex + Age + Sex \times Age + (1|Site) + (1|I), \end{aligned} \tag{5}$$

and the previous model. Models were statistically compared using LRTs (70).
Finally, the LIs (Eq. 1 of left and right brain age predictions for T_1-weighted, diffusion and multimodal MRI (LI_{HBA}, i.e. the asymmetry in brain age predictions) were associated with age, controlling for sex and scanner site as random effect:

$$Age = LI_{HBA} + Sex + (1|Site). \tag{6}$$

The LI_{HBA}s' age-sensitivity was then assessed (as for brain features, see Eqs. 2-3), using LRTs comparing the above model with a baseline model excluding LI_{HBA} (Eq. 3):

$$Age = Sex + (1|Site). \tag{7}$$

Phenotype associations of brain age. In an exploratory analysis step, we assessed association patterns between brain ages and health-and-lifestyle factors which have previously demonstrated an association with brain age (20, 26, 38–41). This analysis step served to compare phenotype associations across estimated brain ages. The health-and-lifestyle factors included alcohol drinking (binary), height and weight supplementing body mass index (BMI), diabetes diagnosis (binary), diastolic blood pressure, systolic blood pressure, pulse pressure, hypertension (binary), cholesterol level (binary), and smoking (binary describing current smokers). For this last analysis step, LMERs were used with the following structure:

$$\begin{aligned} P = BA + Sex + Age + \\ Sex \times Age + (1|Site), \end{aligned} \tag{8}$$

where BA refers brain age incorporating both GBA and HBA, P is the phenotype.
Furthermore, where applicable, we corrected p-values for multiple testing using Bonferroni correction and an α-level of $p < .05$. We used a high-precision approach to calculate exact p-values utilizing the Multiple Precision Floating-Point Reliable R package (71), and report standardized β-values.

DRAFT

Results

Hemispheric differences and age sensitivity for GM and WM features. Paired samples t-tests showed that a significant proportion of the GM and WM features differed between hemispheres with medium effect sizes. Among the significant 793 of 840 dMRI feature asymmetries (94.4%, $p < .05$), the mean effect size was d_{dMRI} = 0.57±0.44. The largest differences were found for DTI FA in the inferior longitudinal fasciculus (d = 3.64), and cingulum (d = 1.95), and for AD in superior longitudinal fasciculus.

Effects sizes of the significant hemispheric differences of the 115 of 117 T_1-weighted features (98.3%), were similar: mean d_{T_1} = 0.53±0.41, and the largest asymmetries were found for the surface area of the transverse-temporal region (d = 1.81), frontal pole (d = 1.76), and pars orbitalis (d = 1.74; see Supplement 12 for T_1-weighted and dMRI features with strongest hemispheric differences).

LRTs comparing a baseline model predicting age from sex and scanner site compared to a model where the respective metric was added indicated most features as age-sensitive (1491 of the 1680 (88.75%) dMRI metrics, and 231 of the 234 (99.15%) T_1-weighted features). Age-sensitivity was strongly expressed in both significant T_1-weighted features (mean F_{T_1} = 1333.93±1897.44), as well as significant dMRI metrics (mean F_{dMRI} = 2310.55±2356.73) with strongest age-sensitivity observed for right hemisphere surface area of the pericalcerine cortex and nucleus accumbens, and the volume of the right putamen, and DTI RD in the right fornix-striaterminalis pathway, and left anterior corona radiata and inferior fronto-occipital fasciculus ($F > 10,063$; see Supplement 13 for features with strongest age sensitivity).

Considering only left/right averages identified only DTI AD, and WMTI axial and radial extra-axonal diffusivity to not differ between hemispheres ($p > .05$). Furthermore, BRIA extra-axonal radial diffusivity extra ($p = 1$) and left WMTI radial extra-axonal diffusivity ($p = .13$) were not age-sensitive using LRTs (Supplement 2). All other left/right averages differed between hemispheres and were age-sensitive. Furthermore, the age-relationships for most of the left/right averages were similar across hemispheres (Figure 1, Supplement 14; both for crude and adjusted values: Supplement 6-7). However, differences in dMRI metrics were observed for the ends of the distribution including individuals aged younger than 55 ($N = 5,307$) and older than 75 ($N = 3,480$).

GM and WM feature asymmetry. Using LRTs identified 80 (68.38%) of the 117 T_1-weighted and 642 of the 840 (76.43%) dMRI LI features as age sensitive ($p < .05$), with the majority of asymmetries being negatively associated with age (Supplement 10). The strongest adjusted relationships between the respective features and age were found for dMRI (mean $|\beta_{dMRI}|$ = 0.08±0.05, mean $|\beta_{T_1}|$ = 0.05±0.03; Figure 2). The largest effects were found for BRIA micro FA, micro RD, and SMTmc extra-neurite transverse microscopic diffusivity in the cingulum (β = -0.29, β = 0.26, β = 0.25), and BRIA cerebrospinal fluid fraction, micro RD, and micro ADC, and and DTI MD and AD in the fornix-striaterminalis pathway (β = -0.24, β = -0.23, β = -0.22, β = -0.24, β = -0.21), and finally SMTmc extra-neurite transverse microscopic diffusivity in the uncinate fasciculus (β = -0.21).

For T_1-weighted metrics, rostro-medial (β = -0.15), lateral (β = -0.10) and medial orbito-frontal cortical thickness LI (β = -0.11) showed the strongest negative associations with age. Inferior parietal thickness (β = 0.17), pallidum volume (β = 0.13), and inferior lateral ventricle volume LI (β = 0.09) showed the strongest positive associations with age. Using left/right averages does detect LI associations with age only with a lower magnitude (Supplement 8-9).

No influences of hemisphere, modality or handedness on brain age estimates. Model performance metrics indicated that most accurately age predictions were accomplished using multimodal MRI data based on left, right, and both hemispheres (Table 1), with obtained HBA and GBA being strongly correlated with each other for similar models (Figure 3).

LMERs did not indicate a difference between modalities (Hypothesis 1) when comparing brain ages estimated from dMRI to multimodal MRI ($p = .623$), and dMRI to T_1-weighted MRI ($p = .452$). There were also no differences in brain age estimates between hemispheres ($p = .413$, Hypothesis 2). Moreover, LRTs indicated no significant difference between models when adding handedness ($\chi^2 = 4.19$, $p = .123$, $df = 2$) or handedness-hemisphere interaction and handedness ($\chi^2 = 7.32$, $p = .120$, $df = 4$; see Eqs. 4-5).

Lower brain age asymmetry at higher ages. To test whether asymmetries between hemisphere-specific brain age predictions, as described by the LI_{HBA}, were lower at higher ages, LI_{HBA} was correlated with age. LI_{HBA} showed negative crude correlations with age for T_1-weighted ($r = -0.301$, $p < .001$), dMRI ($r = -0.719$, $p < .001$), and multimodal models ($r = -0.384$, $p < .001$). The associations were similar when using LMEs adjusting for sex and site (T_1-weighted: $\beta = -0.256$, $p < .001$, dMRI: $\beta = -0.663$, $p < .001$, multimodal: $\beta = -0.338$, $p < .001$). LRTs indicate the age-sensitivity of LI_{HBA} (T_1-weighted: $\chi^2 = 41.19$, $p < .001$, dMRI: $\chi^2 = 276.24$, $p < .001$, multimodal: $\chi^2 = 71.73$, $p < .001$).

HBA and GBA and health-and-lifestyle factors. We further investigated the pattern of relationships with general health-and-lifestyle phenotypes across HBAs (Figure 4). Relationships between brain ages from single and both hemispheres were similar within modalities, but varied slightly between modalities (Supplement 3, 4, 5).

Discussion

In the present work we investigated a new way of utilizing brain age to differentiate between hemispheres, and performed a detailed assessment of brain asymmetry associations with age. As a baseline, we showed that most grey and white matter features were age-sensitive and differed between hemispheres with relatively large effect sizes. Brain

DRAFT

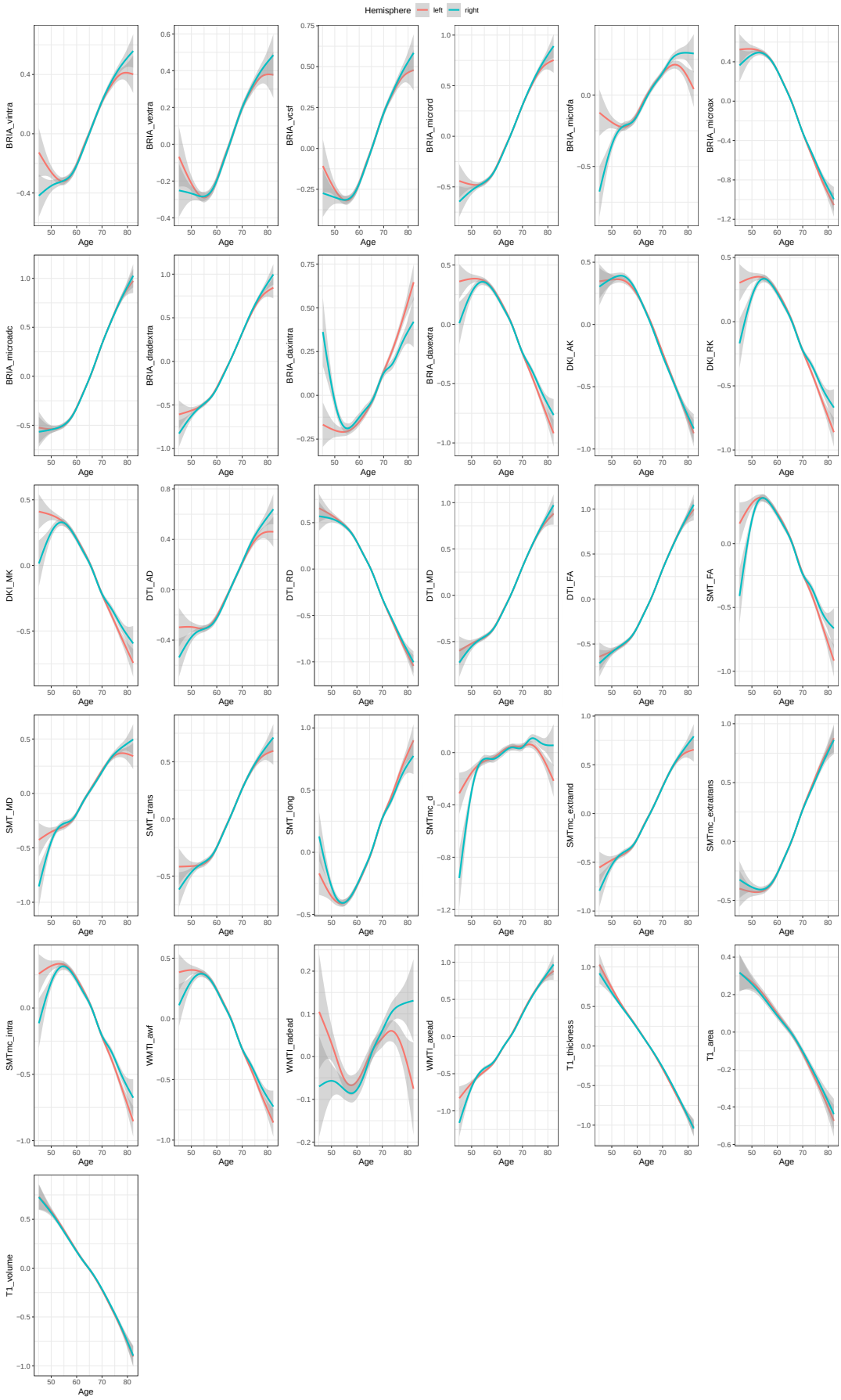

Fig. 1. Standardised mean values of GM and WM features by age per hemisphere. Values are corrected for sex and scanner site. The grey shaded area indicates the 95% CI. BRIA Drad extra in both left and right hemispheres and WMTI radEAD in the left hemisphere were not age-sensitive (see Supplement 9)

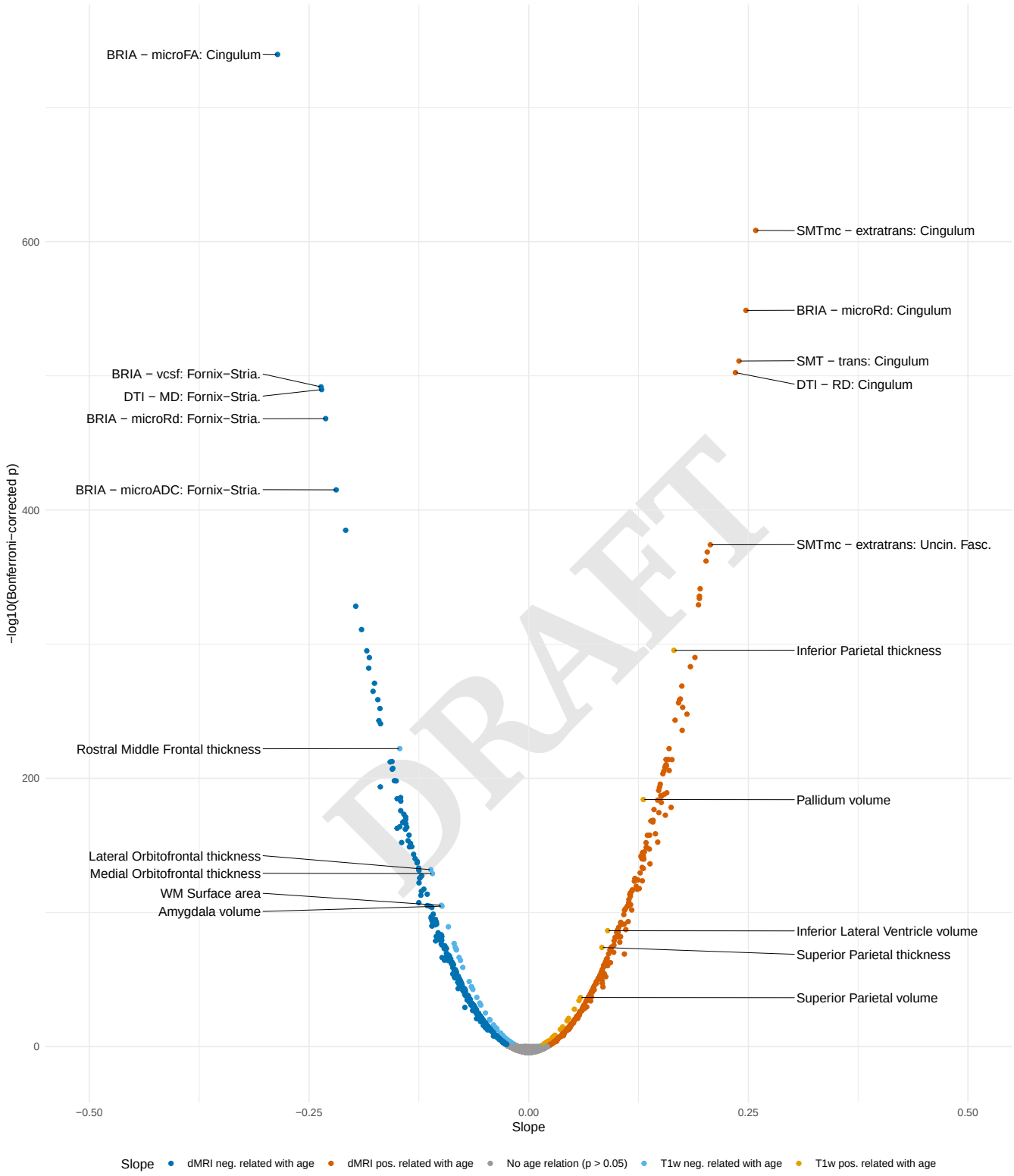

Fig. 2. T_1-weighted and dMRI features asymmetry-age-associations. The plot presents the standardized (sex- and site-corrected) regression slopes versus Bonferroni-adjusted -log10 p-values. Labelling was done separately for T_1-weighted and dMRI indicating the 10 most significantly associated features (five for $\beta > 0$ and five for $\beta < 0$). Uncin. Fasc. = Uncinate Fasciculus, Fornix-Stria. = Fornix-Striaterminalis. Full tables are available at https://github.com/MaxKorbmacher/Hemispheric_Brain_Age/.

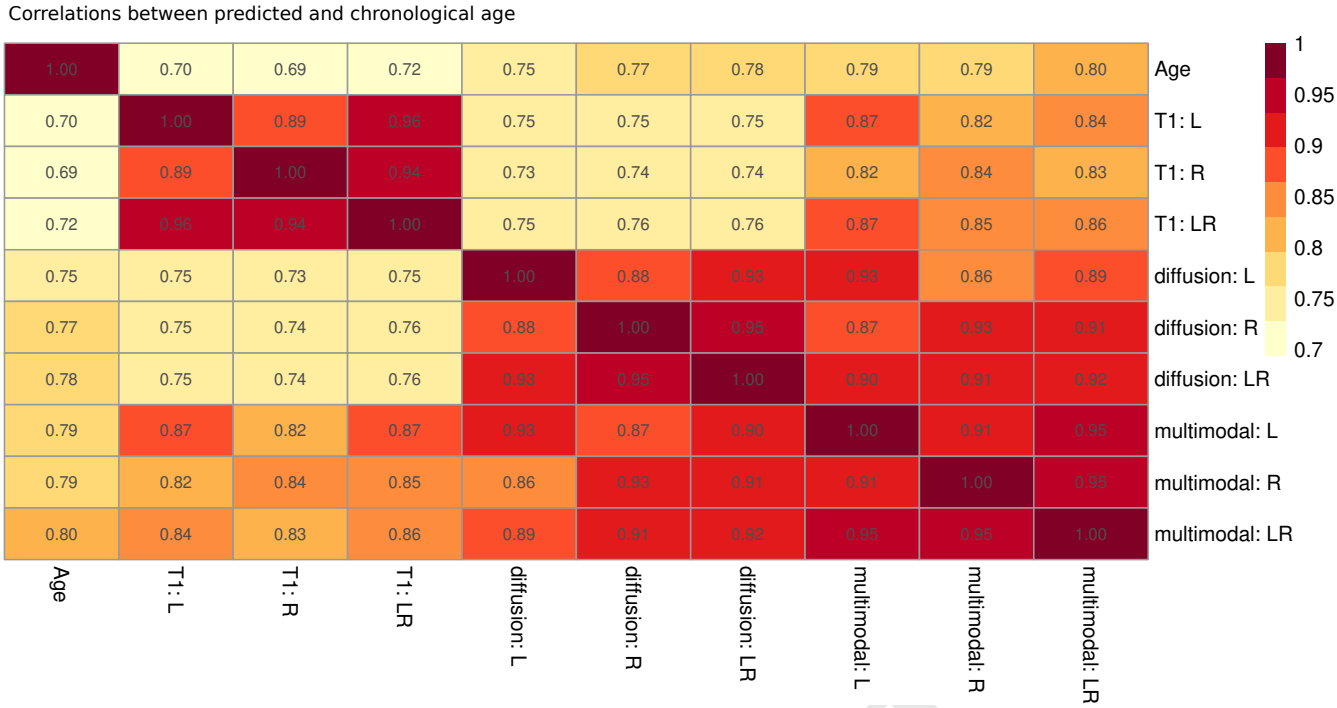

Fig. 3. Pearson correlation coefficients between chronological and predicted ages for T_1-weighted, diffusion, and multimodal MRI for left, right and both hemispheres. All Bonferroni-corrected $p < .001$. L: left hemisphere, R: right hemisphere, LR: both hemispheres.

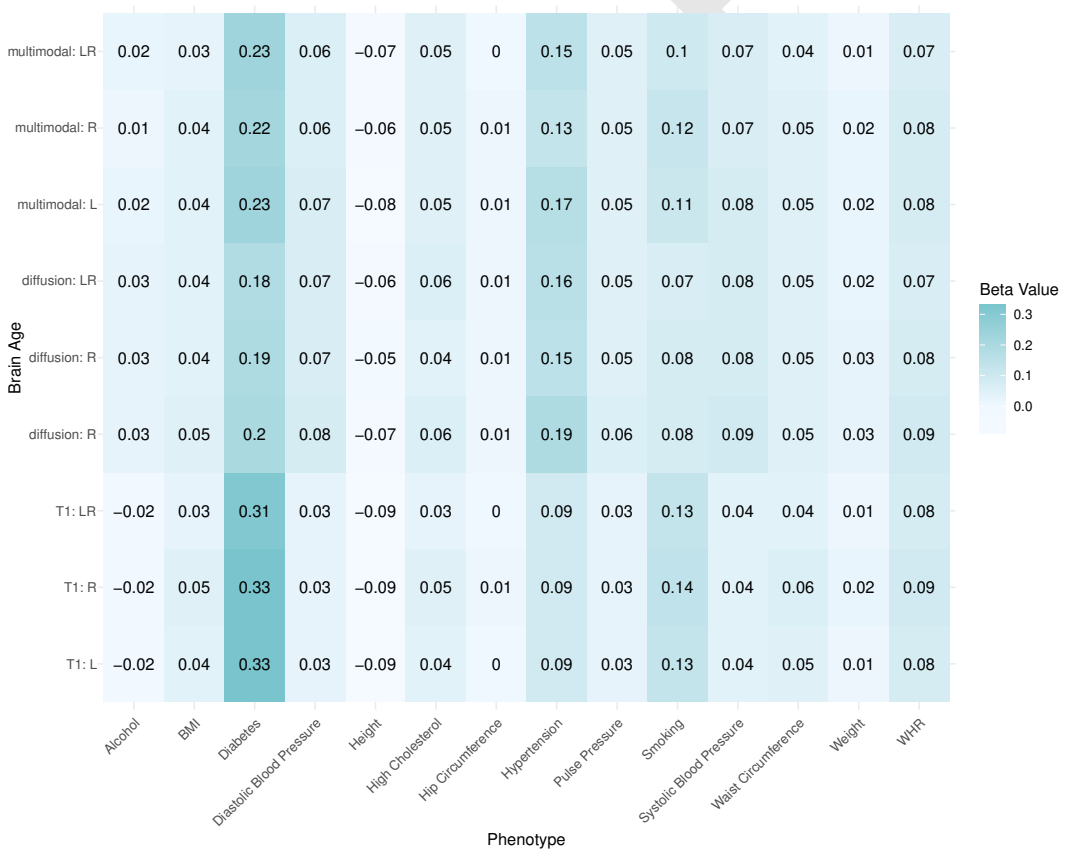

Fig. 4. Association between general health-and-lifestyle phenotypes and brain age estimated from different modalities, left, right and both hemispheres. For simplicity, standardized slopes with $|\beta| < 0.005$ were rounded down to $\beta = 0$. L: left hemisphere, R: right hemisphere, LR: both hemispheres. Note that differences between participants who drink alcohol compared to those who do not drink alcohol were non-significant, and hip circumference was only significantly associated with dMRI-derived brain ages (see Supplement 5).

Table 1. Hemispheric brain age prediction outcomes.

Model	Features	R^2	MAE	RMSE	Raw Correlation*	Corrected Correlation*
Left T_1w	117	0.504 (0.010)	4.389 (0.054)	5.472 (0.061)	0.708 [0.703, 0.712]	0.898 [0.896, 0.900]
Right T_1w	117	0.492 (0.008)	4.439 (0.049)	5.529 (0.051)	0.705 [0.700, 0.709]	0.892 [0.890, 0.894]
T_1w	234	0.526 (0.011)	4.294 (0.050)	5.356 (0.062)	0.725 [0.721, 0.730]	0.895 [0.893, 0.897]
Left dMRI	840	0.568 (0.014)	4.000 (0.047)	4.990 (0.067)	0.757 [0.753, 0.762]	0.902 [0.900, 0.904]
Right dMRI	840	0.582 (0.013)	3.960 (0.052)	4.967 (0.079)	0.766 [0.762, 0.771]	0.900 [0.898, 0.902]
dMRI	1680	0.605 (0.010)	3.867 (0.059)	4.821 (0.094)	0.781 [0.777, 0.785]	0.902 [0.900, 0.904]
Left multimodal	957	0.630 (0.009)	3.757 (0.046)	4.673 (0.047)	0.794 [0.790, 0.797]	0.906 [0.904, 0.908]
Right multimodal	957	0.634 (0.014)	3.723 (0.073)	4.673 (0.092)	0.794 [0.791, 0.798]	0.902 [0.900, 0.904]
Multimodal	1914	0.628 (0.017)	3.663 (0.055)	4.563 (0.077)	0.793 [0.789, 0.797]	0.905 [0.903, 0.907]

R^2 = Variance explained, MAE = Mean Absolute Error, RMSE = Root Mean Squared Error, Values in round parentheses () refer to standard deviations and square brackets [] to 95% confidence interval around correlations (Pearson's r) of uncorrected brain age estimates and chronological age. * Raw correlation refers to the correlation between raw brain age and chronological age, whereas corrected correlation refers to the correlation between corrected predicted age and age, as described in (72).

asymmetry was age-sensitive, and overall lower at higher ages, which was reflected by asymmetries in HBA also decreasing at higher ages. The link between a smaller degree of asymmetry and higher ages was particularly pronounced in fornix-striaterminalis WM. Opposingly, the strongest relationship of age and brain asymmetry was identified in cingulum WM.

Brain age predictions exhibited concordant accuracy within modalities for left, right, and both hemispheres, and concordant associations with health-and-lifestyle factors. The predictions did not differ statistically between hemispheres, modalities, or handedness groups. This suggests that brain age predictions from a single hemisphere closely approximate predictions utilizing data from both hemispheres. However, HBA allows to assess the structural integrity of each hemisphere individually, and to set brain ages from the two hemispheres in relationship to each other providing a general marker of asymmetry. These asymmetries between left/right HBA were smaller at higher age, resembling the age-dependence of WM and GM asymmetry.

Hemispheric differences and asymmetries. We found that the majority of regional and hemisphere-averaged MRI features differed between hemispheres. Both features and asymmetries were age-sensitive indicating that the investigation of asymmetries are useful across ages and MRI modalities.

Interestingly, hemisphere-averaged features' age-associations and HBA of the same modality were similar between hemispheres (Figure 1), and the hemisphere was not a significant predictor of brain age estimated from a particular hemisphere. However, this is not to say that HBA could not sensitively capture brain asymmetries. Just as brain feature's asymmetry, left/right HBA asymmetry showed a strong inverse relationship with age for dMRI and moderate inverse age-relationships for T_1-weighted and multimodal MRI. Hence, left/right HBA differences need to be interpreted considering the observed age group as they are expected to be higher in younger age compared to older age. Moreover, differences between left and right averages were observed in dMRI measures and characterised by a larger variability at the ends of the sample's age distribution, which was not due to smaller sample sizes for these age groups (Figure 1, with the exception of white matter tract integrity metric radial extra-axonal diffusivity). These group-level statistics inform about general markers of asymmetries, namely hemisphere-averaged metrics and HBA, during healthy ageing. Age-relationships of such markers might be different for younger age or clinical groups.

Several studies present evidence for asymmetries in WM (6, 73–76) and GM (4, 9, 77–79). In contrast to these previous studies, for the first time, we examine various metrics supplying information on both WM and GM in a large sample. While we find various differences between hemispheres, age relationships of T_1-weighted and dMRI features were similar between hemispheres using hemispheric averages. Spatially finer-grained examinations revealed more specific patterns of asymmetry in T_1-weighted features, such as GM thickness (9), and dMRI features (73). This is also shown in the present study by stronger age-effects for specific regional asymmetries compared to asymmetries in hemispheric averages (compare Supplement 9 and 10). Age-MRI metric relationships depend, however, on the selected metric, the sample, and the sampling (cross-sectional or longitudinal) (80, 81). For example, previous evidence from T_1-weighted MRI indicates no differences in GM volume between hemispheres (82), but hemispheric differences of cortical thickness and surface area across ageing (4, 9).

The presented age charts of MRI metrics in the current work (Figure 1, Supplement 6-7) provide similar trends to those reported in previous studies observing global age dependencies (19, 21, 83–85). Yet, the stratification between hemispheres when presenting brain features' age dependence is a novel way of presenting brain charts.

We found asymmetries based on GM and WM brain scalar measures. Unimodal studies with smaller, younger samples presented age-dependence of the brain asymmetry during early WM development (76) and adult cortical thickness (9), other T_1-derived metrics (33), and functional network development (5), showed decreasing asymmetries at higher ages.

DRAFT

The results of the present study support this recent evidence across multimodal MRI features in a large sample: asymmetry of cortical thickness, volume, and area were largely negatively related to age (Figure 2, Supplement 9, 13). We extended these findings by providing additional evidence of similar age-dependence in WM asymmetry. This indicates that older brains appear more symmetric than younger brains in the current sample of middle-aged and older adults.

Notably, we identified strong associations between specific brain regions' asymmetry and age. While primarily frontal GM asymmetry based on thickness decreases, and inferior parietal asymmetry increases (as previously shown in (9)), WM asymmetry clearly outlines fornix-striaterminalis asymmetry to decrease and cingulum asymmetry to increase with age (Figure 2). Fornix was previously described as important region for brain age predictions and as strongly age-sensitive parameter (21). It is worth noting that there were observed negative LI-age-associations in fornix, localised by dMRI metrics from BRIA (BRIA-microRd, BRIA-microADC) and DTI metrics (DTI-MD, DTI-AD; see Figure 2). However, limitations of the different diffusion metrics, such as the inability to account for axonal swelling, infection, or crossing fibres (86), makes the interpretation of such decreases in asymmetry difficult. In turn, a series of dMRI approaches was sensitive to asymmetry in the cingulum tract, which is higher at older ages; in particular radial diffusivity, such as SMT and SMTmc transverse (i.e., radial) diffusivity, BRIA-microRd, and DTI-RD. Although speculative, this observation could indicate a relationship between asymmetry and axonal properties during ageing, such as myelination, density, or diameter, in the cingulum, with yet a more general marker (BRIA-microFA) of anisotropy asymmetry decreasing at older ages.

Fornix has been linked to both normal and abnormal ageing (87) as well as neuropsychiatric disorders (88). While a few studies have investigated fornix asymmetry (89), and some evidence suggests fornix asymmetry to be related to epilepsy (90, 91), this topic requires further investigation. Further, cingulum WM microstructure has been reported to differ between hemispheres (92–94). Abnormalities in cingulum asymmetry have been linked to schizophrenia (95–97) and epilepsy (98, 99), and Alzheimer's disease (100). Additionally, the cingulum tract was associated with the antidepressant effects of deep brain stimulation in treatment-resistant depression (101). Thus, future research could regional asymmetries to evaluate such metrics' value for diagnostics and treatment in a range of brain disorders.

Both GM volume, surface, and thickness show asymmetries across studies (1, 3, 4, 9, 82). We identified the lowest degree of asymmetry linked to higher ages in rostro- and orbito-frontal GM thickness, as previously observed and linked to Alzheimer's disease (9). The strongest positive age-relationships for T_1-weighted features were inferiorparietal thickness – also resembling the findings by Roe et al. (9) – and pallidum as well as lateral ventricle volumes. Evidence on role of pallidum asymmetry on ageing and disorders is limited and generally inconclusive when for example relating pallidum volume to obsessive-compulsive disorder and schizophrenia (102). Moreover, ventricular volume increase at higher ages is a known phenomenon (83). However, lifespan changes in ventricular volume asymmetry in relation to symptom and disorder expression requires additional investigations.

Overall, most MRI feature asymmetries were negatively related to age (Supplement 8-10), as well as all LI brain ages. A potential explanation is that structural differences between hemispheres decrease towards older ages. While the current study focused on a healthy sample, an acceleration of this process might be linked neurodegenerative disorders such as Alzheimer's Disease (9).

Hemispheric brain age. Informed by the presented brain asymmetries and their age-dependence, we suggest HBA, indicating the structural integrity of each hemisphere when compared to the chronological age. Moreover, HBA provides a general marker of asymmetry, when setting left/right HBA in relationship to each other. While this added information to conventional GBA is promising, first, the degree to which HBA captures GBA predictions, had to be assessed. This investigation included (1) direct comparisons of HBA and GBA models and their predictions, (2) the influence of covariates of brain age including MRI modality, hemisphere, handedness, and the hemisphere-handedness interaction effect, and (3) a comparison of health-and-lifestyle phenotype-associations with HBA and GBA. Overall, HBA and GBA were highly similar across these dimensions, and the presented evidence suggests HBA as independent of MRI modality, hemisphere, handedness, and the interaction of hemisphere and handedness.

One speculation is that the WM and GM atlas regions used for averaging of the metrics were too large resulting in too coarse averages. As a result, the brain age models could not pick up structure/tissue differences. On the other hand, the choice of hemisphere or modality did not significantly influence age-prediction accuracy. Furthermore, congruently with previous research which combined MRI modalities (27), we found higher prediction accuracy for multimodal compared to unimodal predictions for both HBA and GBA. Our results extend previous findings on conventional brain age by not only estimating brain age from different MRI modalities, but also for each hemisphere separately. Although we did not observe left/right differences in HBA on the group-level, the metric might be informative on the individual-level. For instance, HBA could hold potential in clinical samples by informing about the consistency between the two hemispheres' brain age predictions. Particularly diseases or conditions which affect a single hemisphere, such as unilateral stroke or trauma, might then be sensitively detected, and the integrity of the unaffected hemisphere can be assessed by observing the congruence of HBA (22). Larger discrepancies between HBAs of the same individual might act as a marker of hemisphere-specific brain health imbalance, which may indicate potential pathology.

DRAFT

Conclusion

We identified asymmetries throughout the brain from midlife to older age. These asymmetries appear lower at higher age across WM and GM. This age-dependency of brain asymmetry is reflected by the difference in left/right hemispheric brain age, which is smaller at higher ages. We furthermore identify various regional asymmetries which do not only show age-dependence but which have also been related to various clinical diagnoses. The identified age-relationships of asymmetries provide future opportunities to better understand ageing and disease development.

AUTHOR CONTRIBUTIONS

Max Korbmacher: Study design, Software, Formal analysis, Visualizations, Project administration, Writing—original draft, Writing—review & editing. Ann Marie de Lange: Software, Writing—review & editing. Dennis van der Meer: Software, Writing – review & editing. Arvid Lundervold: Funding acquisition. Eli Eikefjord: Funding acquisition. Dani Beck: Writing—review & editing. Ole A. Andreassen: Writing—review & editing, Funding acquisition. Lars T. Westlye: Writing—review & editing, Funding acquisition. Ivan I. Maximov: Supervision, Study design, Data preprocessing and quality control, Writing—review & editing, Funding acquisition.

ACKNOWLEDGEMENTS

This study has been conducted using UKB data under Application 27412. UKB has received ethics approval from the National Health Service National Research Ethics Service (ref 11/NW/0382). The work was performed on the Service for Sensitive Data (TSD) platform, owned by the University of Oslo, operated and developed by the TSD service group at the University of Oslo IT-Department (USIT). Computations were performed using resources provided by UNINETT Sigma2 – the National Infrastructure for High Performance Computing and Data Storage in Norway. We want to thank Tobias Kaufmann and Torgeir Moberget who processed the T_1-weighted MRI data, and all UKB participants and facilitators who made this research possible.
This research was funded by the Research Council of Norway (#223273); the South-Eastern Norway Regional Health Authority (#2022080); the European Union's Horizon2020 Research and Innovation Programme (CoMorMent project; Grant #847776), and the Swiss National Science Foundation (#PZ00P3_193658).

CONFLICTS OF INTEREST

OAA has received a speaker's honorarium from Lundbeck and is a consultant to Coretechs.ai.

DATA AND CODE AVAILABILITY

All raw data are available from the UKB (www.ukbiobank.ac.uk). Analysis code and extended supplementary files will be made available at the time of publication at https://github.com/MaxKorbmacher/Hemispheric_Brain_Age.

References

1. Nafeesa Nazlee, Gordon D Waiter, and Anca-Larisa Sandu. Age-associated sex and asymmetry differentiation in hemispheric and lobar cortical ribbon complexity across adulthood: A uk biobank imaging study. *Human Brain Mapping*, 44(1):49–65, 2023.
2. Vyacheslav R Karolis, Maurizio Corbetta, and Michel Thiebaut de Schotten. The architecture of functional lateralisation and its relationship to callosal connectivity in the human brain. *Nature communications*, 10(1):1417, 2019.
3. Karin Saltoun, Ralph Adolphs, Lynn K Paul, Vaibhav Sharma, Joern Diedrichsen, BT Thomas Yeo, and Danilo Bzdok. Dissociable brain structural asymmetry patterns reveal unique phenome-wide profiles. *Nature Human Behaviour*, pages 1–18, 2022.
4. Xiang-Zhen Kong, Samuel R Mathias, Tulio Guadalupe, ENIGMA Laterality Working Group, David C Glahn, Barbara Franke, Fabrice Crivello, Nathalie Tzourio-Mazoyer, Simon E Fisher, Paul M Thompson, et al. Mapping cortical brain asymmetry in 17,141 healthy individuals worldwide via the ENIGMA Consortium. *Proceedings of the National Academy of Sciences*, 115(22):E5154–E5163, 2018.
5. Oktay Agcaoglu, R Miller, Andy R Mayer, Kenneth Hugdahl, and Vince D Calhoun. Lateralization of resting state networks and relationship to age and gender. *Neuroimage*, 104: 310–325, 2015.
6. Sebastian Ocklenburg, Patrick Friedrich, Onur Güntürkün, and Erhan Genç. Intrahemispheric white matter asymmetries: the missing link between brain structure and functional lateralization? *Reviews in the Neurosciences*, 27(5):465–480, 2016.
7. Thomas R. Barrick, I. Nigel Lawes, Clare E. Mackay, and Chris A. Clark. White Matter Pathway Asymmetry Underlies Functional Lateralization. *Cerebral Cortex*, 17(3):591–598, 04 2006. ISSN 1047-3211. doi: 10.1093/cercor/bhk004.
8. Tao Sun and Christopher A Walsh. Molecular approaches to brain asymmetry and handedness. *Nature Reviews Neuroscience*, 7(8):655–662, 2006.
9. James M Roe, Didac Vidal-Piñeiro, Øystein Sørensen, Andreas M Brandmaier, Sandra Düzel, Hector A Gonzalez, Rogier A Kievit, Ethan Knights, Simone Kühn, Ulman Lindenberger, et al. Asymmetric thinning of the cerebral cortex across the adult lifespan is accelerated in Alzheimer's disease. *Nature communications*, 12(1):721, 2021.
10. Paul M Thompson, Jason L Stein, Sarah E Medland, Derrek P Hibar, Alejandro Arias Vasquez, Miguel E Renteria, Roberto Toro, Neda Jahanshad, Gunter Schumann, Barbara Franke, et al. The enigma consortium: large-scale collaborative analyses of neuroimaging and genetic data. *Brain imaging and behavior*, 8:153–182, 2014.
11. Peipei Li, Elizabeth Ensink, Sean Lang, Lee Marshall, Meghan Schilthuis, Jared Lamp, Irving Vega, and Viviane Labrie. Hemispheric asymmetry in the human brain and in parkinson's disease is linked to divergent epigenetic patterns in neurons. *Genome biology*, 21 (1):1–23, 2020.
12. Xiang-Zhen Kong, Premika SW Boedhoe, Yoshinari Abe, Pino Alonso, Stephanie H Ameis, Paul D Arnold, Francesca Assogna, Justin T Baker, Marcelo C Batistuzzo, Francesco Benedetti, et al. Mapping cortical and subcortical asymmetry in obsessive-compulsive disorder: findings from the enigma consortium. *Biological psychiatry*, 87(12):1022–1034, 2020.
13. Xiang-Zhen Kong, Merel C Postema, Tulio Guadalupe, Carolien de Kovel, Premika SW Boedhoe, Martine Hoogman, Samuel R Mathias, Daan Van Rooij, Dick Schijven, David C Glahn, et al. Mapping brain asymmetry in health and disease through the enigma consortium. *Human brain mapping*, 43(1):167–181, 2022.
14. Dick Schijven, Merel C Postema, Masaki Fukunaga, Junya Matsumoto, Kenichiro Miura, Sonja MC de Zwarte, Neeltje EM Van Haren, Wiepke Cahn, Hilleke E Hulshoff Pol, René S Kahn, et al. Large-scale analysis of structural brain asymmetries in schizophrenia via the enigma consortium. *Proceedings of the National Academy of Sciences*, 120(14): e2213880120, 2023.
15. Ivan I. Maximov and Lars T. Westlye. Comparison of different neurite density metrics with brain asymmetry evaluation. *Zeitschrift für Medizinische Physik*, 2023. ISSN 0939-3889. doi: https://doi.org/10.1016/j.zemedi.2023.07.003.
16. Siamak Ardekani, Anand Kumar, George Bartzokis, and Usha Sinha. Exploratory voxel-based analysis of diffusion indices and hemispheric asymmetry in normal aging. *Magnetic resonance imaging*, 25(2):154–167, 2007.
17. Katja Franke and Christian Gaser. Ten years of brainage as a neuroimaging biomarker of brain aging: what insights have we gained? *Frontiers in neurology*, page 789, 2019.
18. Tobias Kaufmann, Dennis van der Meer, Nhat Trung Doan, Emanuel Schwarz, Martina J Lund, Ingrid Agartz, Dag Alnæs, Deanna M Barch, Ramona Baur-Streubel, Alessandro Bertolino, et al. Common brain disorders are associated with heritable patterns of apparent aging of the brain. *Nature neuroscience*, 22(10):1617–1623, 2019.
19. Dani Beck, Ann-Marie G de Lange, Ivan I Maximov, Geneviève Richard, Ole A Andreassen, Jan E Nordvik, and Lars T Westlye. White matter microstructure across the adult lifespan: A mixed longitudinal and cross-sectional study using advanced diffusion models and brain-age prediction. *NeuroImage*, 224:117441, 2021.
20. Dani Beck, Ann-Marie G De Lange, Dag Alnæs, Ivan I Maximov, Mads L Pedersen, Olof Dahlqvist Leinhard, Jennifer Linge, Rozalyn Simon, Geneviève Richard, Kristine M Ulrichsen, et al. Adipose tissue distribution from body MRI is associated with cross-sectional and longitudinal brain age in adults. *NeuroImage: Clinical*, 33:102949, 2022.
21. Max Korbmacher, Ann Marie de Lange, Dennis van der Meer, Dani Beck, Eli Eikefjord, Arvid Lundervold, Ole A Andreassen, Lars T Westlye, and Ivan I Maximov. Brain-wide associations between white matter and age highlight the role of fornix microstructure in brain ageing. *Human brain mapping*, 44(10), 2023.
22. Geneviève Richard, Knut Kolskår, Kristine M Ulrichsen, Tobias Kaufmann, Dag Alnæs, Anne-Marthe Sanders, Erlend S Dørum, Jennifer Monereo Sánchez, Anders Petersen, Hege Ihle-Hansen, et al. Brain age prediction in stroke patients: Highly reliable but limited sensitivity to cognitive performance and response to cognitive training. *NeuroImage: Clinical*, 25:102159, 2020.
23. Ann-Marie G de Lange, Claudia Barth, Tobias Kaufmann, Melis Anatürk, Sana Suri, Klaus P Ebmeier, and Lars T Westlye. The maternal brain: Region-specific patterns of brain aging are traceable decades after childbirth. *Human Brain Mapping*, 41(16):4718–4729, 2020.
24. Irene Voldsbekk, Claudia Barth, Ivan I Maximov, Tobias Kaufmann, Dani Beck, Genevieve Richard, Torgeir Moberget, Lars T Westlye, and Ann-Marie G de Lange. A history of previous childbirths is linked to women's white matter brain age in midlife and older age. *Human Brain Mapping*, 42(13):4372–4386, 2021.
25. Geneviève Richard, Knut Kolskår, Anne-Marthe Sanders, Tobias Kaufmann, Anders Petersen, Nhat Trung Doan, Jennifer Monereo Sánchez, Dag Alnæs, Kristine M Ulrichsen, Erlend S Dørum, et al. Assessing distinct patterns of cognitive aging using tissue-specific brain age prediction based on diffusion tensor imaging and brain morphometry. *PeerJ*, 6: e5908, 2018.
26. James H Cole. Multimodality neuroimaging brain-age in uk biobank: relationship to biomedical, lifestyle, and cognitive factors. *Neurobiology of aging*, 92:34–42, 2020.
27. Ann-Marie G De Lange, Melis Anatürk, Sana Suri, Tobias Kaufmann, James H Cole, Ludovica Griffanti, Enikő Zsoldos, Daria EA Jensen, Nicola Filippini, Archana Singh-Manoux, et al. Multimodal brain-age prediction and cardiovascular risk: The Whitehall II MRI sub-study. *NeuroImage*, 222:117292, 2020.
28. Catriona D Good, Ingrid Johnsrude, John Ashburner, Richard NA Henson, Karl J Friston, and Richard SJ Frackowiak. Cerebral asymmetry and the effects of sex and handedness on brain structure: a voxel-based morphometric analysis of 465 normal adult human brains. *Neuroimage*, 14(3):685–700, 2001.
29. Han Jang, Jae Youn Lee, Kang Il Lee, and Kang Min Park. Are there differences in brain morphology according to handedness? *Brain and behavior*, 7(7):e00730, 2017.
30. Sebastian Ocklenburg, Dorothea Metzen, Caroline Schlüter, Christoph Fraenz, Larissa Arning, Fabian Streit, Onur Güntürkün, Robert Kumsta, and Erhan Genç. Polygenic scores for handedness and their association with asymmetries in brain structure. *Brain Structure and Function*, pages 1–13, 2021.
31. Miguel E Rentería. Cerebral asymmetry: a quantitative, multifactorial, and plastic brain phenotype. *Twin Research and Human Genetics*, 15(3):401–413, 2012.
32. RR Benson, DB FitzGerald, LL LeSueur, DN Kennedy, KK Kwong, BR Buchbinder, TL Davis, RM Weisskoff, TM Talavage, WJ Logan, et al. Language dominance determined

DRAFT

by whole brain functional mri in patients with brain lesions. *Neurology*, 52(4):798–798, 1999.
33. Camille Michèle Williams, Hugo Peyre, Roberto Toro, and Franck Ramus. Comparing brain asymmetries independently of brain size. *NeuroImage*, 254:119118, 2022.
34. Robert J Jirsaraie, Tobias Kaufmann, Vishnu Bashyam, Guray Erus, Joan L Luby, Lars T Westlye, Christos Davatzikos, Deanna M Barch, and Aristeidis Sotiras. Benchmarking the generalizability of brain age models: challenges posed by scanner variance and prediction bias. *Human Brain Mapping*, 44(3):1118–1128, 2023.
35. Max Korbmacher, Meng-Yun Wang, Rune Eikeland, Ralph Buchert, Ole A. Andreassen, Thomas Espeseth, Esten Leonardsen, Lars T. Westlye, Ivan I. Maximov, and Karsten Specht. Considerations on brain age predictions from repeatedly sampled data across time. *Brain and Behavior*, (in-press). doi: https://doi.org/10.1002/brb3.3219.
36. Brian A Nosek, Charles R Ebersole, Alexander C DeHaven, and David T Mellor. The preregistration revolution. *Proceedings of the National Academy of Sciences*, 115(11): 2600–2606, 2018.
37. Brian A Nosek, Emorie D Beck, Lorne Campbell, Jessica K Flake, Tom E Hardwicke, David T Mellor, Anna E van't Veer, and Simine Vazire. Preregistration is hard, and worthwhile. *Trends in cognitive sciences*, 23(10):815–818, 2019.
38. Dani Beck, Ann-Marie G de Lange, Mads L Pedersen, Dag Alnæs, Ivan I Maximov, Irene Voldsbekk, Geneviève Richard, Anne-Marthe Sanders, Kristine M Ulrichsen, Erlend S Dørum, et al. Cardiometabolic risk factors associated with brain age and accelerate brain ageing. *Human brain mapping*, 43(2):700–720, 2022.
39. Max Korbmacher, Tiril P Gurholt, Ann-Marie G de Lange, Dennis van der Meer, Dani Beck, Eli Eikefjord, Arvid Lundervold, Ole A Andreassen, Lars T Westlye, and Ivan I Maximov. Bio-psycho-social factors' associations with brain age: a large-scale uk biobank diffusion study of 35,749 participants. *Frontiers in Psychology*, 14:1117732, 2023.
40. Esten H Leonardsen, Han Peng, Tobias Kaufmann, Ingrid Agartz, Ole A Andreassen, Elisabeth Gulowsen Celius, Thomas Espeseth, Hanne F Harbo, Einar A Høgestøl, Ann-Marie De Lange, et al. Deep neural networks learn general and clinically relevant representations of the ageing brain. *NeuroImage*, 256:119210, 2022.
41. Stephen M Smith, Lloyd T Elliott, Fidel Alfaro-Almagro, Paul McCarthy, Thomas E Nichols, Gwenaëlle Douaud, and Karla L Miller. Brain aging comprises many modes of structural and functional change with distinct genetic and biophysical associations. *elife*, 9:e52677, 2020.
42. Fidel Alfaro-Almagro, Mark Jenkinson, Neal K Bangerter, Jesper LR Andersson, Ludovica Griffanti, Gwenaëlle Douaud, Stamatios N Sotiropoulos, Saad Jbabdi, Moises Hernandez-Fernandez, Emmanuel Vallee, et al. Image processing and quality control for the first 10,000 brain imaging datasets from uk biobank. *Neuroimage*, 166:400–424, 2018.
43. Ivan I Maximov, Dennis van Der Meer, Ann-Marie G de Lange, Tobias Kaufmann, Alexey Shadrin, Oleksandr Frei, Thomas Wolfers, and Lars T Westlye. Fast qualitY conTrol meThod foR derIved diffUsion Metrics (YTTRIUM) in big data analysis: UK Biobank 18,608 example. *Human brain mapping*, 42(10):3141–3155, 2021.
44. Adon FG Rosen, David R Roalf, Kosha Ruparel, Jason Blake, Kevin Seelaus, Lakshmi P Villa, Rastko Ciric, Philip A Cook, Christos Davatzikos, Mark A Elliott, et al. Quantitative assessment of structural image quality. *Neuroimage*, 169:407–418, 2018.
45. Zhou Wang, Alan C Bovik, Hamid R Sheikh, and Eero P Simoncelli. Image quality assessment: from error visibility to structural similarity. *IEEE transactions on image processing*, 13(4):600–612, 2004.
46. Dominique Brunet, Edward R Vrscay, and Zhou Wang. On the mathematical properties of the structural similarity index. *IEEE Transactions on Image Processing*, 21(4):1488–1499, 2011.
47. Karla L Miller, Fidel Alfaro-Almagro, Neal K Bangerter, David L Thomas, Essa Yacoub, Junqian Xu, Andreas J Bartsch, Saad Jbabdi, Stamatios N Sotiropoulos, Jesper LR Andersson, et al. Multimodal population brain imaging in the UK Biobank prospective epidemiological study. *Nature neuroscience*, 19(11):1523–1536, 2016.
48. Cathie Sudlow, John Gallacher, Naomi Allen, Valerie Beral, Paul Burton, John Danesh, Paul Downey, Paul Elliott, Jane Green, Martin Landray, et al. UK biobank: an open access resource for identifying the causes of a wide range of complex diseases of middle and old age. *PLoS medicine*, 12(3):e1001779, 2015.
49. Jelle Veraart, Els Fieremans, and Dmitry S Novikov. Diffusion MRI noise mapping using random matrix theory. *Magnetic resonance in medicine*, 76(5):1582–1593, 2016.
50. Elias Kellner, Bibek Dhital, Valerij G Kiselev, and Marco Reisert. Gibbs-ringing artifact removal based on local subvoxel-shifts. *Magnetic resonance in medicine*, 76(5):1574–1581, 2016.
51. Jesper LR Andersson and Stamatios N Sotiropoulos. An integrated approach to correction for off-resonance effects and subject movement in diffusion MR imaging. *Neuroimage*, 125:1063–1078, 2016.
52. Stephen M Smith, Mark Jenkinson, Mark W Woolrich, Christian F Beckmann, Timothy EJ Behrens, Heidi Johansen-Berg, Peter R Bannister, Marilena De Luca, Ivana Drobnjak, David E Flitney, et al. Advances in functional and structural MR image analysis and implementation as FSL. *Neuroimage*, 23:S208–S219, 2004.
53. Mark Jenkinson, Christian F Beckmann, Timothy EJ Behrens, Mark W Woolrich, and Stephen M Smith. FSL. *Neuroimage*, 62(2):782–790, 2012.
54. Peter J Basser, James Mattiello, and Denis LeBihan. Mr diffusion tensor spectroscopy and imaging. *Biophysical journal*, 66(1):259–267, 1994.
55. Jens H Jensen, Joseph A Helpern, Anita Ramani, Hanzhang Lu, and Kyle Kaczynski. Diffusional kurtosis imaging: the quantification of non-gaussian water diffusion by means of magnetic resonance imaging. *Magnetic Resonance in Medicine: An Official Journal of the International Society for Magnetic Resonance in Medicine*, 53(6):1432–1440, 2005.
56. Els Fieremans, Jens H Jensen, and Joseph A Helpern. White matter characterization with diffusional kurtosis imaging. *Neuroimage*, 58(1):177–188, 2011.
57. Enrico Kaden, Frithjof Kruggel, and Daniel C Alexander. Quantitative mapping of the per-axon diffusion coefficients in brain white matter. *Magnetic resonance in medicine*, 75(4): 1752–1763, 2016.
58. Enrico Kaden, Nathaniel D Kelm, Robert P Carson, Mark D Does, and Daniel C Alexander. Multi-compartment microscopic diffusion imaging. *NeuroImage*, 139:346–359, 2016.
59. Marco Reisert, Elias Kellner, Bibek Dhital, Juergen Hennig, and Valerij G Kiselev. Disentangling micro from mesostructure by diffusion MRI: a Bayesian approach. *Neuroimage*, 147:964–975, 2017.
60. Bruce Fischl. Freesurfer. *Neuroimage*, 62(2):774–781, 2012.
61. Anders M Dale, Bruce Fischl, and Martin I Sereno. Cortical surface-based analysis: I. Segmentation and surface reconstruction. *Neuroimage*, 9(2):179–194, 1999.
62. Stephen M Smith, Mark Jenkinson, Heidi Johansen-Berg, Daniel Rueckert, Thomas E Nichols, Clare E Mackay, Kate E Watkins, Olga Ciccarelli, M Zaheer Cader, Paul M Matthews, et al. Tract-based spatial statistics: voxelwise analysis of multi-subject diffusion data. *Neuroimage*, 31(4):1487–1505, 2006.
63. Stephen M Smith. Fast robust automated brain extraction. *Human brain mapping*, 17(3): 143–155, 2002.
64. S Mori, S Wakana, LM Nagae-Poetscher, and PCM Van Zijl. MRI atlas of human white matter. *American Journal of Neuroradiology*, 27(6):1384, 2006.
65. Kegang Hua, Jiangyang Zhang, Setsu Wakana, Hangyi Jiang, Xin Li, Daniel S Reich, Peter A Calabresi, James J Pekar, Peter CM van Zijl, and Susumu Mori. Tract probability maps in stereotaxic spaces: analyses of white matter anatomy and tract-specific quantification. *Neuroimage*, 39(1):336–347, 2008.
66. Rahul S Desikan, Florent Ségonne, Bruce Fischl, Brian T Quinn, Bradford C Dickerson, Deborah Blacker, Randy L Buckner, Anders M Dale, R Paul Maguire, Bradley T Hyman, et al. An automated labeling system for subdividing the human cerebral cortex on MRI scans into gyral based regions of interest. *Neuroimage*, 31(3):968–980, 2006.
67. Tianqi Chen and Carlos Guestrin. Xgboost: A scalable tree boosting system. In *Proceedings of the 22nd acm sigkdd international conference on knowledge discovery and data mining*, pages 785–794, 2016.
68. Ann-Marie G de Lange and James H Cole. Commentary: Correction procedures in brain-age prediction. *NeuroImage: Clinical*, 26, 2020.
69. Ann-Marie G de Lange, Melis Anatürk, Jaroslav Rokicki, Laura KM Han, Katja Franke, Dag Alnæs, Klaus P Ebmeier, Bogdan Draganski, Tobias Kaufmann, Lars T Westlye, et al. Mind the gap: Performance metric evaluation in brain-age prediction. *Human Brain Mapping*, 43 (10):3113–3129, 2022.
70. Erich L Lehmann. On likelihood ratio tests. *Selected works of EL Lehmann*, pages 209–216, 2012.
71. Martin Maechler, Maintainer Martin Maechler, SystemRequirementsNote MPFR, MASS Suggests, and MASS SuggestsNote. Package 'rmpfr'. 2016.
72. Ann-Marie G de Lange, Tobias Kaufmann, Dennis van der Meer, Luigi A Maglanoc, Dag Alnæs, Torgeir Moberget, Gwenaëlle Douaud, Ole A Andreassen, and Lars T Westlye. Population-based neuroimaging reveals traces of childbirth in the maternal brain. *Proceedings of the National Academy of Sciences*, 116(44):22341–22346, 2019.
73. C Büchel, T Raedler, M Sommer, M Sach, C Weiller, and MA Koch. White matter asymmetry in the human brain: a diffusion tensor MRI study. *Cerebral cortex*, 14(9):945–951, 2004.
74. Remika Mito, David Raffelt, Thijs Dhollander, David N Vaughan, J-Donald Tournier, Olivier Salvado, Amy Brodtmann, Christopher C Rowe, Victor L Villemagne, and Alan Connelly. Fibre-specific white matter reductions in Alzheimer's disease and mild cognitive impairment. *Brain*, 141(3):888–902, 01 2018. ISSN 0006-8950. doi: 10.1093/brain/awx355.
75. H Takao, N Hayashi, and K Ohtomo. White matter asymmetry in healthy individuals: a diffusion tensor imaging study using tract-based spatial statistics. *Neuroscience*, 193: 291–299, 2011.
76. Jae W. Song, Paul D. Mitchell, James Kolasinski, P. Ellen Grant, Albert M. Galaburda, and Emi Takahashi. Asymmetry of White Matter Pathways in Developing Human Brains. *Cerebral Cortex*, 25(9):2883–2893, 05 2014. ISSN 1047-3211. doi: 10.1093/cercor/bhu084.
77. Kexin Huang, Yafei Kang, Zhongcheng Wu, Yubo Wang, Suping Cai, and Liyu Huang. Asymmetrical alterations of grey matter among psychiatric disorders: a systematic analysis by voxel-based activation likelihood estimation. *Progress in Neuro-Psychopharmacology and Biological Psychiatry*, 110:110322, 2021.
78. Arthur W Toga and Paul M Thompson. Mapping brain asymmetry. *Nature Reviews Neuroscience*, 4(1):37–48, 2003.
79. Christine Chiarello, David Vazquez, Adam Felton, and Alessandra McDowell. Structural asymmetry of the human cerebral cortex: Regional and between-subject variability of surface area, cortical thickness, and local gyrification. *Neuropsychologia*, 93:365–379, 2016.
80. Maria A Di Biase, Ye Ella Tian, Richard AI Bethlehem, Jakob Seidlitz, Aaron F Alexander-Bloch, BT Thomas Yeo, and Andrew Zalesky. Mapping human brain charts cross-sectionally and longitudinally. *Proceedings of the National Academy of Sciences*, 120 (20):e2216798120, 2023.
81. Katherine S Button, John PA Ioannidis, Claire Mokrysz, Brian A Nosek, Jonathan Flint, Emma SJ Robinson, and Marcus R Munafò. Power failure: why small sample size undermines the reliability of neuroscience. *Nature reviews neuroscience*, 14(5):365–376, 2013.
82. Yasuyuki Taki, Benjamin Thyreau, Shigeo Kinomura, Kazunori Sato, Ryoi Goto, Ryuta Kawashima, and Hiroshi Fukuda. Correlations among brain gray matter volumes, age, gender, and hemisphere in healthy individuals. *PloS one*, 6(7):e22734, 2011.
83. Richard AI Bethlehem, Jakob Seidlitz, Simon R White, Jacob W Vogel, Kevin M Anderson, Chris Adamson, Sophie Adler, George S Alexopoulos, Evdokia Anagnostou, Ariosky Areces-Gonzalez, et al. Brain charts for the human lifespan. *Nature*, 604(7906):525–533, 2022.
84. Yongbin Wei, Han Zhang, and Yong Liu. Charting Normative Brain Variability Across the Human Lifespan. *Neuroscience Bulletin*, 39(2):362–364, 2023.
85. Lars T Westlye, Kristine B Walhovd, Anders M Dale, Atle Bjørnerud, Paulina Due-Tønnessen, Andreas Engvig, Håkon Grydeland, Christian K Tamnes, Ylva Østby, and Anders M Fjell. Life-span changes of the human brain white matter: diffusion tensor imaging (DTI) and volumetry. *Cerebral cortex*, 20(9):2055–2068, 2010.
86. Wim Van Hecke, Louise Emsell, Stefan Sunaert, et al. *Diffusion tensor imaging: a practical handbook*. Springer, 2016.
87. Derek B Archer, Kurt Schilling, Niranjana Shashikumar, Varuna Jasodanand, Elizabeth Moore, Kimberly Pechman, Murat Bilgel, Lori Beason-Held, Yang An, Andrea Shafer, et al.

DRAFT

Leveraging longitudinal diffusion mri data to quantify differences in white matter microstructural decline in normal and abnormal aging. *bioRxiv*, pages 2023–05, 2023.

88. Ya-Nan Ou, Yi-Jun Ge, Bang-Sheng Wu, Yi Zhang, Yu-Chao Jiang, Kevin Kuo, Liu Yang, Lan Tan, Jian-Feng Feng, Wei Cheng, et al. The genetic architecture of fornix white matter microstructure and their involvement in neuropsychiatric disorders. *Translational Psychiatry*, 13(1):180, 2023.
89. Uta N Sboto-Frankenstein, Tiffany Lazar, R Bruce Bolster, Sunny Thind, Patricia Dreessen de Gervai, Marco LH Gruwel, Stephen D Smith, and Boguslaw Tomanek. Symmetry of the fornix using diffusion tensor imaging. *Journal of Magnetic Resonance Imaging*, 40(4):929–936, 2014.
90. Ruben Kuzniecky, E Bilir, F Gilliam, E Faught, R Martin, and J Hugg. Quantitative mri in temporal lobe epilepsy: evidence for fornix atrophy. *Neurology*, 53(3):496–496, 1999.
91. Luis Concha, Christian Beaulieu, and Donald W Gross. Bilateral limbic diffusion abnormalities in unilateral temporal lobe epilepsy. *Annals of neurology*, 57(2):188–196, 2005.
92. Rene J Huster, Rene Westerhausen, Frank Kreuder, Elisabeth Schweiger, and Werner Wittling. Morphologic asymmetry of the human anterior cingulate cortex. *Neuroimage*, 34 (3):888–895, 2007.
93. Aaron Kucyi, Massieh Moayedi, Irit Weissman-Fogel, Mojgan Hodaie, and Karen D Davis. Hemispheric asymmetry in white matter connectivity of the temporoparietal junction with the insula and prefrontal cortex. *PloS one*, 7(4):e35589, 2012.
94. Jue Wang, Dong-Qiang Liu, Han Zhang, Wei-Xuan Zhu, Zhang-Ye Dong, and Yu-Feng Zang. Asymmetry of the dorsal anterior cingulate cortex: evidences from multiple modalities of mri. *Neuroinformatics*, 11:149–157, 2013.
95. Tsutomu Takahashi, Yasuhiro Kawasaki, Kenzo Kurokawa, Hirofumi Hagino, Shigeru Nohara, Ikiko Yamashita, Kazue Nakamura, Masahiko Murata, Mie Matsui, Michio Suzuki, et al. Lack of normal structural asymmetry of the anterior cingulate gyrus in female patients with schizophrenia: a volumetric magnetic resonance imaging study. *Schizophrenia Research*, 55(1-2):69–81, 2002.
96. Dara S Manoach, G Avinash Ketwaroo, Frida E Polli, Katharine N Thakkar, Jason JS Barton, Donald C Goff, Bruce Fischl, Mark Vangel, and David S Tuch. Reduced microstructural integrity of the white matter underlying anterior cingulate cortex is associated with increased saccadic latency in schizophrenia. *Neuroimage*, 37(2):599–610, 2007.
97. Sung Woo Joo, Myong-Wuk Chon, Yogesh Rathi, Martha E Shenton, Marek Kubicki, and Jungsun Lee. Abnormal asymmetry of white matter tracts between ventral posterior cingulate cortex and middle temporal gyrus in recent-onset schizophrenia. *Schizophrenia Research*, 192:159–166, 2018.
98. Xu Zhao, Zhi-qiang Zhou, Ying Xiong, Xu Chen, Ke Xu, Juan Li, Ying Hu, Xiao-long Peng, and Wen-zhen Zhu. Reduced interhemispheric white matter asymmetries in medial temporal lobe epilepsy with hippocampal sclerosis. *Frontiers in Neurology*, 10:394, 2019.
99. Yiwei Zhang, Zhaoxi Liu, Wanchen Dou, Juan Wei, Yuelei Lv, Bo Hou, Hui You, and Feng Feng. Study of the microstructure of brain white matter in medial temporal lobe epilepsy based on diffusion tensor imaging. *Brain and Behavior*, 13(4):e2919, 2023.
100. Danqing Xiao, Kesheng Wang, Luke Theriault, Elhelou Charbel, and Alzheimer's Disease Neuroimaging Initiative. White matter integrity and key structures affected in alzheimer's disease characterized by diffusion tensor imaging. *European Journal of Neuroscience*, 56(8):5319–5331, 2022.
101. Giulia Cattarinussi, Hossein Sanjari Moghaddam, Mohammad Hadi Aarabi, Letizia Squarcina, Fabio Sambataro, Paolo Brambilla, and Giuseppe Delvecchio. White matter microstructure associated with the antidepressant effects of deep brain stimulation in treatment-resistant depression: A review of diffusion tensor imaging studies. *International Journal of Molecular Sciences*, 23(23):15379, 2022.
102. Yi Wang, Yong-Ming Wang, Simon SY Lui, and Raymond CK Chan. Clinical implication of brain asymmetries in psychiatric disorders. *Biological Psychiatry*, 87(12):1014–1016, 2020.

DRAFT

Supplementary Note 1: Tuned Hyperparameters

Overview of the tuned hyperparameters for each of the used brain age models.

Modality	Hemisphere	Learning Rate	Maximum Depth	Number of Trees
Multimodal	Both	0.1	8	140
Multimodal	Left	0.05	7	180
Multimodal	Right	0.1	8	140
dMRI	Both	0.1	6	100
dMRI	Left	0.1	4	180
dMRI	Right	0.1	5	180
T_1w	Both	0.1	5	140
T_1w	Left	0.1	6	140
T_1w	Right	0.1	6	180

Supplementary Note 2: Global Metrics' Age Sensitivity

LRTs outcomes testing global metrics' age sensitivity using Eqs. (2-3), with p-values being Bonferroni-corrected for multiple comparison. Acronyms lh and rh refer to mean left and right hemisphere, respectively.

Metric	Sum of Squares	F	p	Metric	Sum of Squares	F	p
BRIA_vintra_lh	-14143.51	256.78	<.001	*DTI_MD_rh*	-294821.39	6256.88	<.001
BRIA_vintra_rh	-13492.91	244.88	<.001	*DTI_FA_lh*	-294054.08	6237.71	<.001
BRIA_vextra_lh	-8868.68	160.58	<.001	*DTI_FA_rh*	-290846.08	6157.77	<.001
BRIA_vextra_rh	-8247.91	149.29	<.001	*SMT_FA_lh*	-96237.02	1824.32	<.001
BRIA_vcsf_lh	-12339.56	223.82	<.001	*SMT_FA_rh*	-88924.97	1679.10	<.001
BRIA_vcsf_rh	-11691.20	211.99	<.001	*SMT_MD_lh*	-145717.99	2837.80	<.001
BRIA_micrord_lh	-110749.44	2115.93	<.001	*SMT_MD_rh*	-138236.90	2681.03	<.001
BRIA_micrord_rh	-112757.19	2156.64	<.001	*SMT_trans_lh*	-236947.06	4859.34	<.001
BRIA_microfa_lh	-7389.49	133.69	<.001	*SMT_trans_rh*	-230976.33	4720.50	<.001
BRIA_microfa_rh	-7660.08	138.61	<.001	*SMT_long_lh*	-233251.22	4773.28	<.001
BRIA_microax_lh	-20330.95	370.29	<.001	*SMT_long_rh*	-221802.60	4509.03	<.001
BRIA_microax_rh	-19217.81	349.82	<.001	*SMTmc_d_lh*	-12811.82	232.44	<.001
BRIA_microadc_lh	-244852.70	5044.67	<.001	*SMTmc_d_rh*	-15325.44	278.40	<.001
BRIA_microadc_rh	-242965.40	5000.27	<.001	*SMTmc_extramd_lh*	-234164.26	4794.51	<.001
BRIA_dradextra_lh	-0.87	0.02	1.00	*SMTmc_extramd_rh*	-221755.78	4507.96	<.001
BRIA_dradextra_rh	-0.56	0.01	1.00	*SMTmc_extratrans_lh*	-269921.51	5643.84	<.001
BRIA_daxintra_lh	-45776.98	844.85	<.001	*SMTmc_extratrans_rh*	-251971.27	5213.02	<.001
BRIA_daxintra_rh	-32572.59	597.02	<.001	*SMTmc_intra_lh*	-162286.59	3189.66	<.001
BRIA_daxextra_lh	-33941.70	622.56	<.001	*SMTmc_intra_rh*	-138122.05	2678.64	<.001
BRIA_daxextra_rh	-29058.51	531.64	<.001	*WMTI_awf_lh*	-216212.24	4381.26	<.001
DKI_AK_lh	-98394.96	1867.39	<.001	*WMTI_awf_rh*	-198966.98	3992.24	<.001
DKI_AK_rh	-107687.41	2054.02	<.001	*WMTI_radead_lh*	-538.93	9.72	0.11
DKI_RK_lh	-134762.36	2608.66	<.001	*WMTI_radead_rh*	-1786.25	32.22	<.001
DKI_RK_rh	-117109.00	2245.17	<.001	*WMTI_axead_lh*	-15537.30	282.28	<.001
DKI_MK_lh	-166559.26	3281.46	<.001	*WMTI_axead_rh*	-140593.59	2730.28	<.001
DKI_MK_rh	-146629.45	2856.99	<.001	*T1_lh_thickness*	-361976.02	7460.14	<.001
DTI_AD_lh	-6414.25	115.99	<.001	*T1_rh_thickness*	-337720.79	6873.27	<.001
DTI_AD_rh	-32682.00	599.06	<.001	*T1_lh_area*	-131984.99	2428.71	<.001
DTI_RD_lh	-103169.79	1963.06	<.001	*T1_rh_area*	-115500.16	2109.17	<.001
DTI_RD_rh	-98654.94	1872.59	<.001	*T1_lh_volume*	-366138.06	7562.34	<.001
DTI_MD_lh	-296264.43	6292.97	<.001	*T1_rh_volume*	-351072.41	7194.50	<.001

DRAFT

Supplementary Note 3: Unstandardized beta values of associations between brain ages and health-and-lifestyle factors

The table presents the slopes of the association between brain ages (columns 2-10) and different health-and-lifestyle phenotypes (column 1). For a colour-coded visualisation of these beta values see Figure 4.

Associated Phenotype	LT1	RT1	bothT1	LdMRI	RdMRI	bothdMRI	Lmulti	Rmulti	Both multi
Waist Circumference	0.02	0.02	0.02	0.02	0.02	0.02	0.02	0.02	0.02
Hip Circumference	0.00	0.01	0.00	0.01	0.01	0.01	0.00	0.00	0.00
Height	-0.05	-0.05	-0.05	-0.04	-0.03	-0.04	-0.05	-0.04	-0.04
BMI	0.05	0.06	0.04	0.06	0.05	0.05	0.05	0.05	0.05
Weight	0.00	0.01	0.00	0.01	0.01	0.01	0.01	0.01	0.01
WHR	4.95	5.51	4.94	5.41	5.36	4.97	5.41	5.58	5.13
Diastolic Blood Pressure	0.02	0.02	0.02	0.04	0.04	0.04	0.04	0.04	0.04
Systolic Blood Pressure	0.01	0.01	0.01	0.03	0.02	0.02	0.02	0.02	0.02
Pulse Pressure	0.01	0.01	0.01	0.02	0.02	0.02	0.02	0.02	0.02
Diabetes	1.73	1.76	1.69	1.08	1.09	1.05	1.36	1.29	1.38
Hypertension	0.46	0.49	0.48	1.04	0.87	0.91	0.96	0.79	0.89
High Cholesterol	0.20	0.25	0.18	0.35	0.26	0.33	0.31	0.27	0.30
Alcohol	-0.09	-0.09	-0.10	0.17	0.16	0.16	0.09	0.05	0.10
Smoking	0.69	0.77	0.70	0.44	0.47	0.40	0.66	0.73	0.58

DRAFT

Supplementary Note 4: t-values of associations between brain ages and health-and-lifestyle factors

Associated Phenotype	LT_1w	RT_1w	$bothT_1w$	LdMRI	RdMRI	bothdMRI	Lmulti	Rmulti	Both multi
Waist Circumference	10.66	12.84	10.03	13.68	13.24	12.16	12.56	12.95	11.51
Hip Circumference	0.66	2.86	0.02	3.83	3.31	2.77	1.55	2.00	0.96
Height	-16.51	-15.53	-16.58	-13.93	-10.24	-12.11	-16.32	-13.17	-14.64
BMI	9.89	11.93	8.95	12.82	11.31	10.88	11.36	11.04	10.33
Weight	2.92	5.26	2.01	6.24	6.62	5.38	4.20	5.31	3.92
WHR	16.15	17.37	15.86	18.24	17.93	16.76	18.49	18.70	17.45
Diastolic Blood Pressure	7.63	7.28	7.92	21.74	19.51	19.00	18.94	18.00	18.15
Systolic Blood Pressure	9.81	9.74	9.93	23.31	20.26	20.90	20.64	19.44	20.51
Pulse Pressure	7.28	7.45	7.21	14.47	12.13	13.35	13.07	12.18	13.49
Diabetes	11.40	11.17	10.91	7.32	7.31	7.12	9.38	8.69	9.44
Hypertension	9.13	9.39	9.48	21.38	17.73	18.66	20.07	16.23	18.41
High Cholesterol	3.25	3.86	2.94	5.78	4.26	5.60	5.34	4.55	5.10
Alcohol	-1.15	-1.10	-1.14	2.17	1.93	1.99	1.14	0.66	1.25
Smoking	5.59	5.98	5.54	3.66	3.84	3.37	5.53	6.04	4.88

The table presents the t-values of the association between brain ages (columns 2-10) and different health-and-lifestyle phenotypes (column 1). Prefix L-, R- or both means left, right and whole brain values were in use.

Supplementary Note 5: P-values of associations between brain ages and health-and-lifestyle factors

Associated Phenotype	LT_1w	RT_1w	$bothT_1w$	LdMRI	RdMRI	bothdMRI	Lcombi	Rcombi	bothcombi
Waist Circumference	<.001	<.001	<.001	<.001	<.001	<.001	<.001	<.001	<.001
Hip Circumference	.508	.004	.987	<.001	<.001	<.001	.006	.120	.046
Height	<.001	<.001	<.001	<.001	<.001	<.001	<.001	<.001	<.001
BMI	<.001	<.001	<.001	<.001	<.001	<.001	<.001	<.001	<.001
Weight	<.001	<.001	<.001	<.001	<.001	<.001	<.001	<.001	<.001
WHR	<.001	<.001	<.001	<.001	<.001	<.001	<.001	<.001	<.001
Diastolic Blood Pressure	<.001	<.001	<.001	<.001	<.001	<.001	<.001	<.001	<.001
Systolic Blood Pressure	<.001	<.001	<.001	<.001	<.001	<.001	<.001	<.001	<.001
Pulse Pressure	<.001	<.001	<.001	<.001	<.001	<.001	<.001	<.001	<.001
Diabetes	<.001	<.001	<.001	<.001	<.001	<.001	<.001	<.001	<.001
Hypertension	<.001	<.001	<.001	<.001	<.001	<.001	<.001	<.001	<.001
High Cholesterol	<.001	<.001	<.001	<.001	<.001	<.001	<.001	<.001	<.001
Alcohol	.249	.273	.255	.030	.053	.047	.255	.255	.508
Smoking	<.001	<.001	<.001	<.001	<.001	<.001	<.001	<.001	<.001

DRAFT

The table presents the p-values of the association between brain ages (columns 2-10) and different health-and-lifestyle phenotypes (column 1).

Supplementary Note 6: Uncorrected mean values' age curves (z-standardised values)

Crude age curves for mean values of grey and white and grey matter features by age per hemisphere.

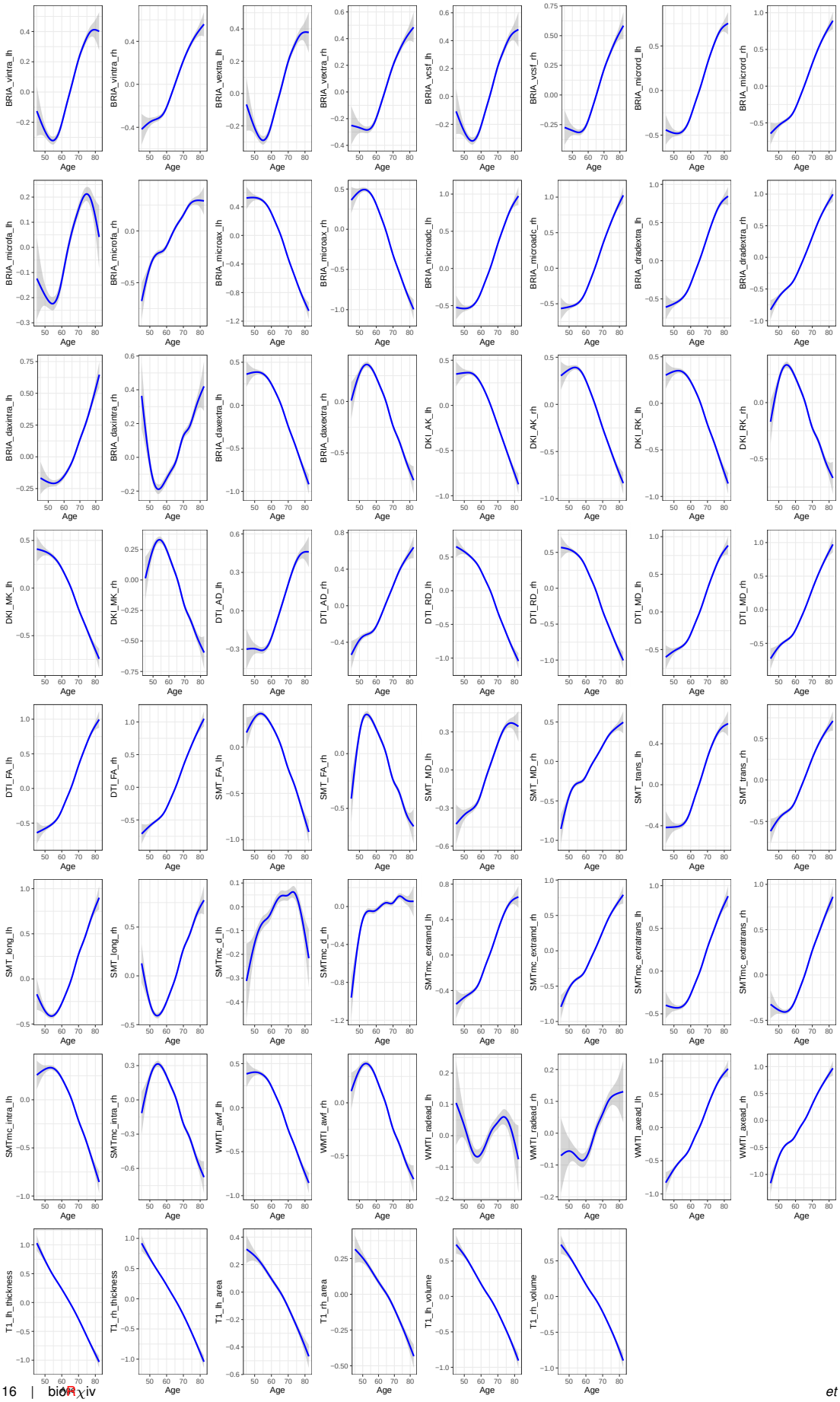

Supplementary Note 7: Corrected mean values' age curves (z-standardised values)

Sex- and site corrected age curves for mean values of grey and white and grey matter features by age per hemisphere.

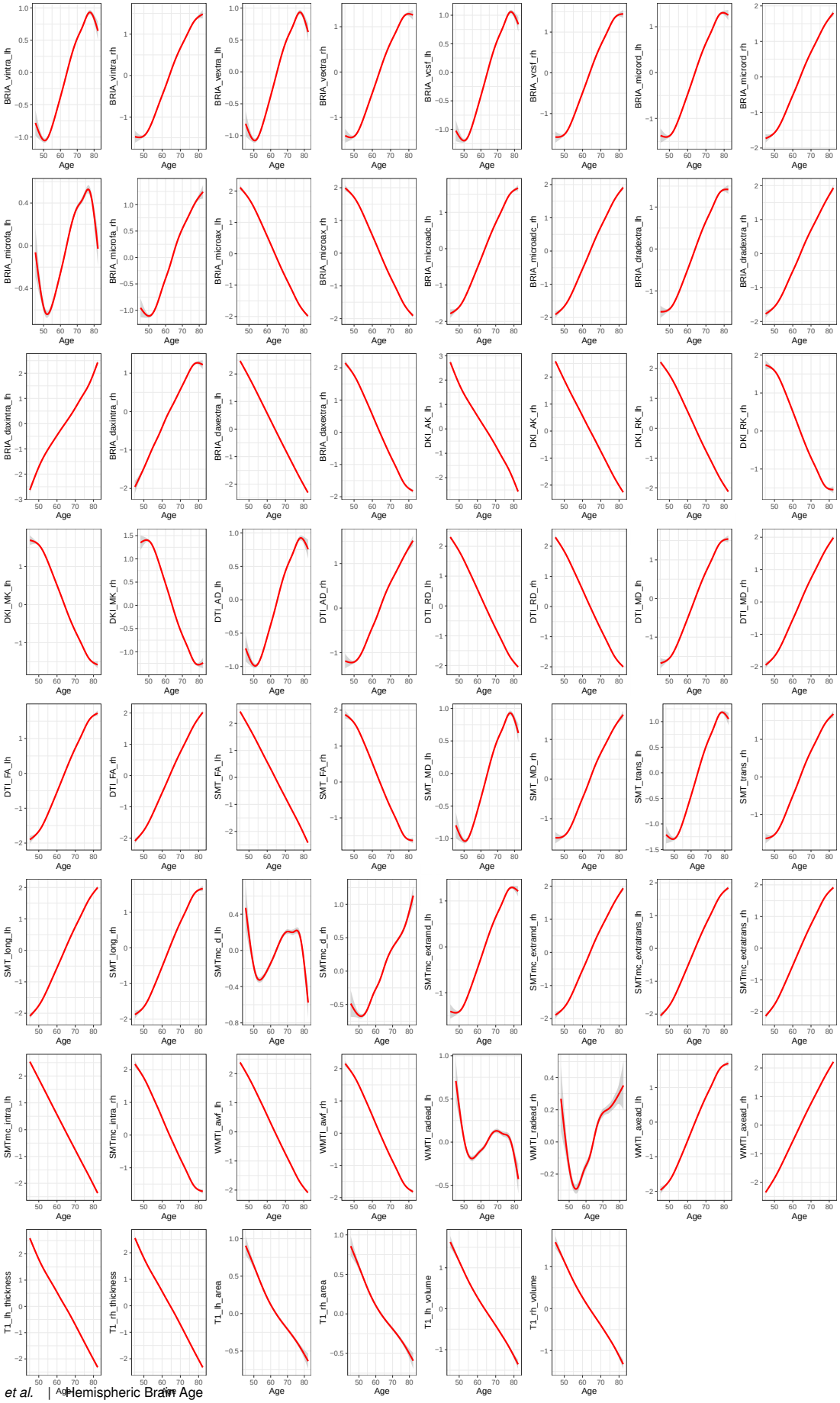

Supplementary Note 8: Laterality indexed hemispheric mean values of grey and white matter features by age.

Outliers defined by Mean±3SD were removed for visualisation purposes.

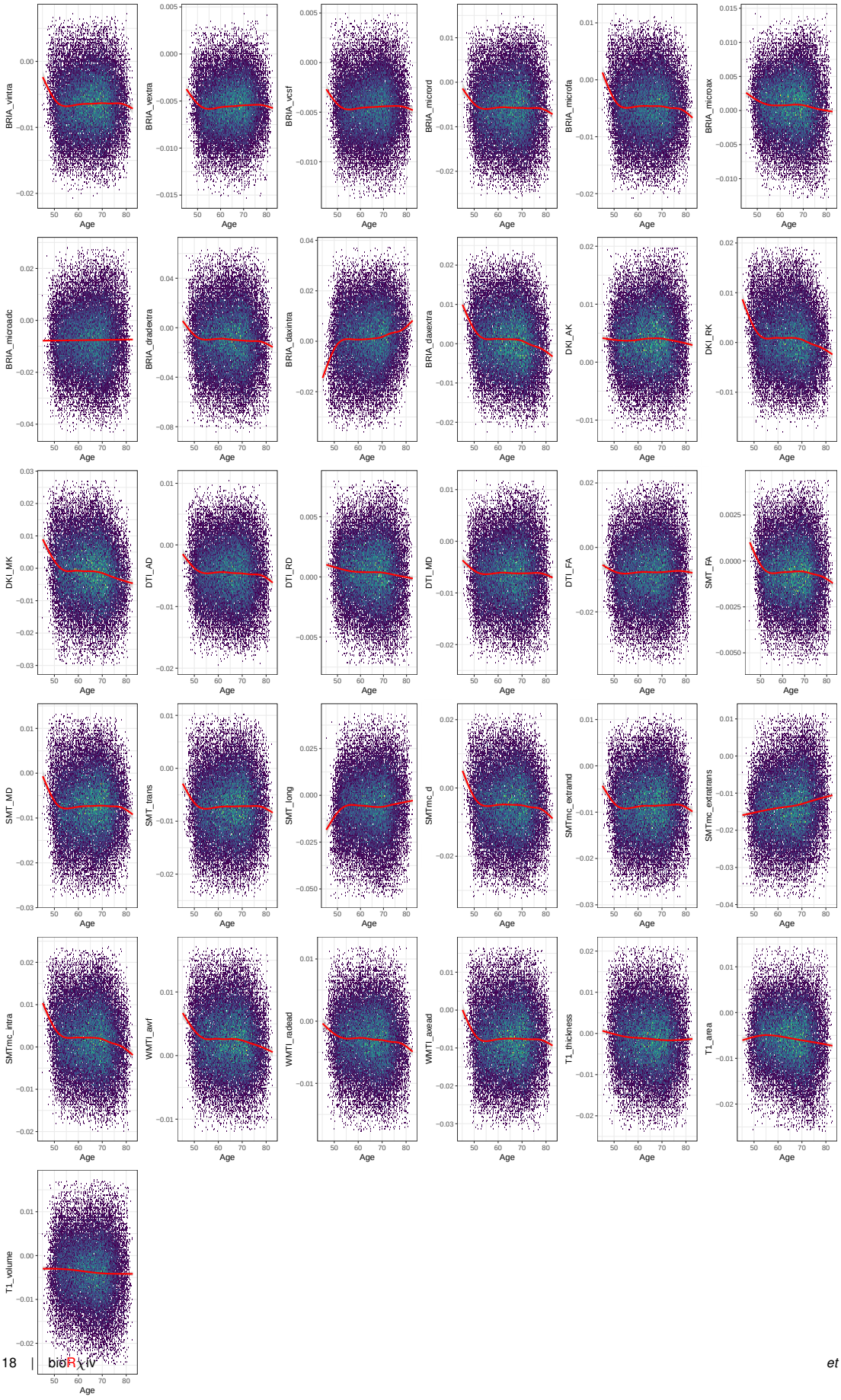

Supplementary Note 9: Age sensitivity of hemispheric mean values of laterality indexed grey and white matter.

Of the presented 31 LI hemispheric mean features, 21 (67.74%) were age sensitive ($p_{Bonferroni} < .05$).

Feature	Beta	Adjusted p-values
BRIA_vintra	0.012	0.462
BRIA_vextra	0.007	1.000
BRIA_vcsf	0.006	1.000
BRIA_micrord	0.012	0.649
BRIA_microfa	-0.006	1.000
BRIA_microax	-0.012	0.560
BRIA_microadc	0.026	<.001
BRIA_dradextra	-0.010	1.000
BRIA_daxintra	0.068	<.001
BRIA_daxextra	-0.018	0.009
DKI_AK	0.025	<.001
DKI_RK	-0.086	<.001
DKI_MK	-0.102	<.001
DTI_AD	-0.007	1.000
DTI_RD	-0.054	<.001
DTI_MD	0.022	0.001
DTI_FA	0.037	<.001
SMT_FA	-0.022	0.001
SMT_MD	0.015	0.121
SMT_trans	0.026	<.001
SMT_long	0.027	<.001
SMTmc_d	-0.030	<.001
SMTmc_extramd	0.042	<.001
SMTmc_extratrans	0.099	<.001
SMTmc_intra	-0.083	<.001
WMTI_awf	-0.072	<.001
WMTI_radead	-0.016	0.049
WMTI_axead	0.008	1.000
T1_thickness	-0.040	<.001
T1_area	-0.097	<.001
T1_volume	-0.056	<.001

DRAFT

Supplementary Note 10: Most significantly age-related laterality indexed grey and white matter features and the distribution of their slopes.

The three panels show the distributions of slopes for sex and scanner site corrected significant associations (at Bonferroni-corrected $p < .05$) between age and laterality indexed grey and white matter features. Panels separate between (1) T_1-weighted features only ($n = 80$ of original $n = 117$), (2) diffusion-weighted features only ($n = 604$ of original $n = 840$), (3) and hemisphere-averaged (multimodal) features ($n = 21$ of total $n = 31$).

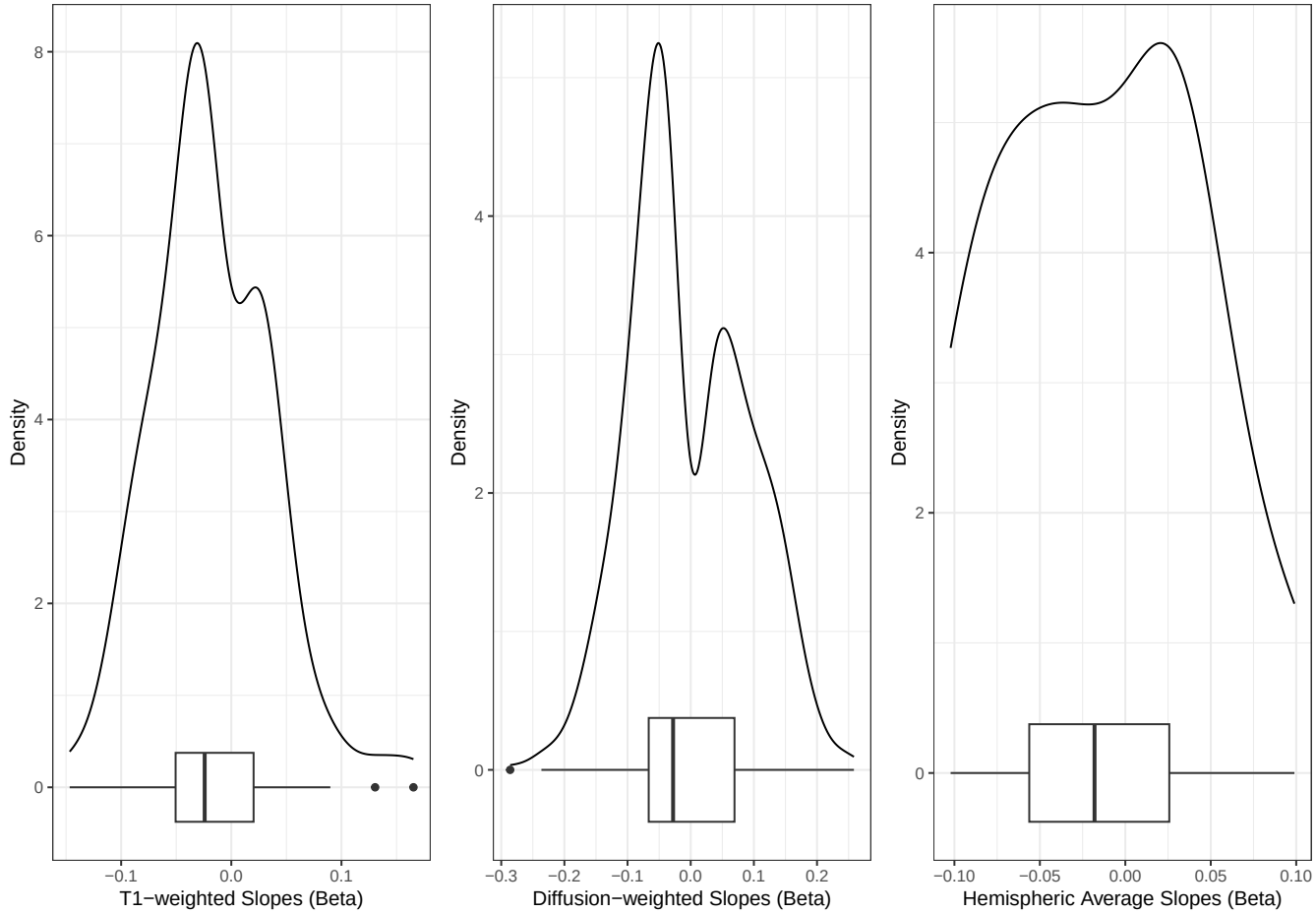

Supplementary Note 11: Description of white matter features by diffusion approaches.

Diffusion Approach	Metrics
Bayesian Rotationally Invariant Approach (BRIA) (59)	intra-axonal axial diffusivity (DAX intra)
	extra-axonal radial diffusivity (DRAD extra)
	microscopic fractional anisotropy (micro FA)
	extra-axonal axial diffusivity (DAX extra)
	intra-axonal water fraction (V intra)
	extra-axonal water fraction (V extra)
	cerebrospinal fluid fraction (vCSF)
	microscopical axial diffusivity (micro AX)
	microscopic radial diffusivity (micro RD)
	microscopical apparent diffusion coefficient (micro ADC)
Diffusion Kurtosis Imaging (DKI) (55, 56)	mean kurtosis (MK)
	radial kurtosis (RK)
	axial kurtosis (AK)
Diffusion Tensor Imaging (DTI) (54)	fractional anisotropy (FA)
	axial diffusivity (AD)
	mean diffusivity (MD)
	radial diffusivity (RD)
Spherical Mean Technique (SMT) (57)	fractional anisotropy (SMT FA)
	mean diffusivity (SMT md)
	transverse diffusion coefficient (SMT trans)
	longitudinal diffusion coefficient (SMT long)
Multi-compartment Spherical Mean Technique (SMTmc) (58)	extra-neurite microscopic mean diffusivity (SMTmc extra md)
	extra-neurite transverse microscopic diffusivity (SMTmc extra trans)
	mc SMTdiffusion coefficient (SMT mcd)
	intra-neurite volume fraction (SMTmc intra)
White Matter Tract Integrity (WMTI) (56)	axonal water fraction (AWF)
	radial extra-axonal diffusivity (radEAD)
	axial extra-axonal diffusivity (axEAD)

DRAFT

Supplementary Note 12: Differences of T_1w and dMRI features between hemispheres.

The table shows the ten largest regional differences between left and right hemispheres' T_1w and dMRI data indicated by effect size (Cohen's d). Bonferroni-adjusted p-values were $p < 2 \times 10^{-308}$.

For full tables see the files Hemi_dMRI_features_diff.csv and Hemi_T1w_features_diff.csv at https://github.com/MaxKorbmacher/Hemispheric_Brain_Age.

T_1-weighted MRI			diffusion MRI		
Feature	**T-value**	**Cohen's d**	**Feature**	**T-value**	**Cohen's d**
Transversetemporal_area	397.45	1.81	DTI.FA_ILF	725.48	3.64
Frontalpole_area	-386.34	1.76	DTI.AD_SLFT	-444.89	2.23
Parsorbitalis_area	-380.71	1.74	DTI.FA_Cingulumcingulategyrus	388.09	1.95
Inferiorparietal_area	-368.85	1.68	DKI.RK_Cingulumcingulategyrus	375.36	1.89
Inferiorparietal_volume	-352.95	1.61	SMT_mc.smt_mc_diff_SLFT	-369.19	1.85
Frontalpole_volume	-340.08	1.55	SMT_mc.smt_mc_extratrans_Cerebralpeduncle	-367.31	1.84
Middletemporal_area	-297.79	1.36	DKI.RK_SLFT	-364.52	1.83
Thalamus.Proper	296.93	1.35	WMTI.awf_Cingulumcingulategyrus	364.46	1.83
Transversetemporal_volume	292.04	1.33	SMT.long_SLFT	-359.08	1.80
Parsorbitalis_volume	-280.74	1.28	DTI.AD_ILF	353.43	1.78

Supplementary Note 13: Age sensitivity of T_1w and diffusion MRI features.

The table shows the ten largest age-effects of regional T_1-weighted and diffusion MRI features sorted after F-values from model comparisons (Likelihood Ratio tests) between a null model explaining age from sex and scanner site and a model adding the respective feature to the null model. Both uncorrected and Bonferroni-adjusted p-values were $p < 2 \times 10^{-308}$.

T_1-weighted MRI			**diffusion MRI**		
Feature	**Sum of Squares**	**F-value**	**Feature**	**Sum of Squares**	**F-value**
rh_pericalcarine_area	-480010.76	10522.57	DTI.RD_Fornix_StriaterminalisR	-568838.72	13114.24
rh_Putamen	-463315.33	10063.63	DTI.FA_AnteriorcoronaradiataL	-554045.66	12664.20
rh_Accumbens.area	-388473.65	8105.49	DTI.FA_IFOFL	-527205.85	11866.98
rh_CortexVol	-353221.31	7235.64	DTI.FA_Fornix_StriaterminalisR	-526713.03	11852.57
lh_postcentral_area	-352105.54	7208.63	DTI.RD_AnteriorcoronaradiataL	-504149.35	11201.30
rh_precentral_area	-339426.44	6903.83	DTI.RD_AnteriorcoronaradiataR	-500047.51	11084.67
rh_rostralanteriorcingulate_area	-336178.66	6826.39	DTI.FA_AnteriorcoronaradiataR	-481860.37	10573.93
rh_transversetemporal_area	-307559.03	6154.98	BRIA.micro_Rd_ATRR	-480010.76	10522.57
lh_Lateral.Ventricle	-297230.83	5917.42	DTI.RD_IFOFL	-471710.65	10293.35
lh_supramarginal_thickness	-276232.45	5441.97	DTI.FA_IFOFR	-470227.52	10252.62

DRAFT

Supplementary Note 14: Mean values of grey and white and grey matter features by age per hemisphere.
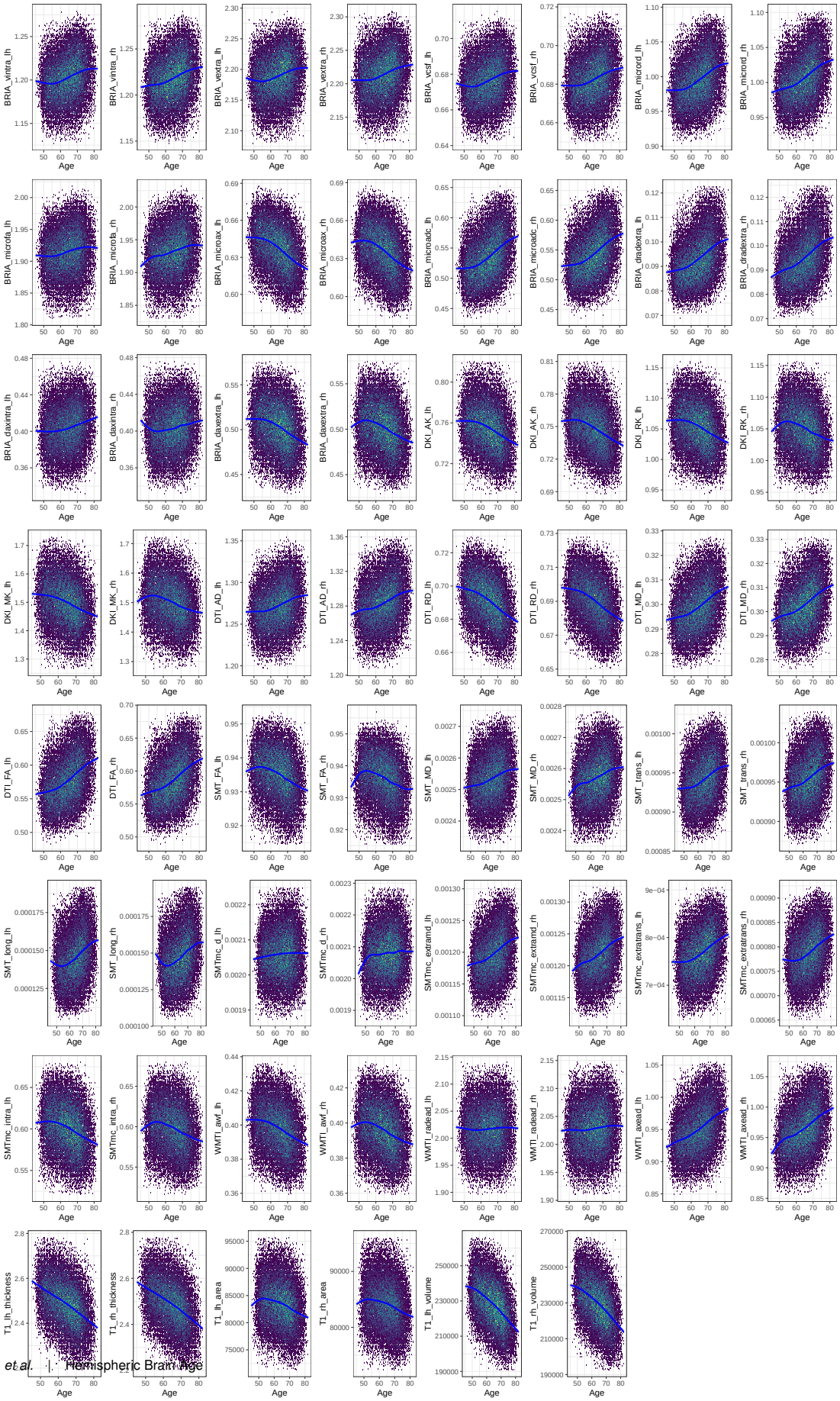
Outliers defined by Mean±3SD were removed for visualisation purposes.